Oil & Natural Gas Technology

DOE Award No.: DE-NT0006553

Progress Report
Second Quarter 2009

ConocoPhillips Gas Hydrate Production Test

Submitted by:
ConocoPhillips
700 G Street
Anchorage, AK 99501
Principle Investigator: David Schoderbek

Prepared for:
United States Department of Energy
National Energy Technology Laboratory

August 28, 2009

Office of Fossil Energy

Disclaimer

Executive Summary

Accomplishments

- Continued the process to gain working interest co-owner approval for the proposed production test sites.
- Chartered, initiated work on the Experimental Design and Well Design Teams.
- Completed laboratory experiments and petrophysical studies which provide data for the production test.

Current Status

- Experimental Design and Well Design work is well underway.
- Work continues to finalize the site of the production test.

Introduction

Work began on the ConocoPhillips Gas Hydrates Production Test (DE-NT0006553) on October 1, 2008. This report is the third quarterly report for the project and summarizes project activities from April 1, 2009 to June 30, 2009. While work continues on Tasks 3 & 4 from Phase 1, Site Identification, this quarter marks the beginning of Phase 2, Field Test Planning.

The report begins with a summary of current Site Identification and Field Test Planning activities. Following this summary is a discussion of three laboratory and petrophysical studies: Role of Free Water in Hydrate Reformation & Permeability, Predicting Methane Hydrate Saturation with the Stanford University Rock Physics Lab Code, and Petrophysical Evaluation of Potential Hydrate-Bearing Wells on the North Slope of Alaska. The full reports from these three studies are included in the appendix.

Site Identification

As presented in the First Quarter, 2009 Progress Report, consensus was reached at the April 3rd Site Selection Workshop that five sites in the Prudhoe Bay and Kuparuk River

units were acceptable production test sites. Work to complete Tasks 2 & 3 from Phase 1, Site Identification, continued in the 2nd Quarter as follows:

Task 2 – Identification, Evaluation, and Selection of Sites for Field Activity
Detailed seismic interpretation of hydrate-bearing sandstones is underway at each of the top five candidate sites Seismically mappable targets vary from site to site, as summarized below:.

	Seismically Mappable Targets
Locale	Hydrate-bearing sandstones
PBU L-106	Upper C, Lower C, D, & E sands
PBU W Kup 3-11-11	Upper C, D, & E sands
PBU NWE2-01	Upper C & D sands
KRU W Sak 24	B sand
PBU Kup St 7-11-12	D sand

Analysis of stacking of hydrate-bearing sandstone targets will support re-ranking of the top-five sites. Based on mapping around KRU W Sak 24 pad and PBU L-pad, well designs including vertical (from ice pad) and short-offset directional (from gravel) are being evaluated.

Task 3 – Field Site Ownership Partner Negotiations
ConocoPhillips continues its efforts to gain permission from Unit co-owners for the field sites identified under Subtask 2.6. ConocoPhillips will continue to keep DOE informed of progress on co-owner negotiations through regular project communications and will inform DOE of any issues within the discussions that could affect the intended content of the production test planned under this project.

Field Test Planning

Two interdisciplinary teams were chartered in the 2nd Quarter to begin work on Task 5, Field Test Planning.

Experimental Design Team

The Experimental Design Team's goal is to ensure that adequate and appropriate data are gathered during the course of drilling, completion and flow testing such that both injectivity and CO_2/CH_4 exchange mechanism can be verified.

The team is led by David Schoderbek, the Project lead, and includes representatives from ConocoPhillips' Reservoir Mechanisms, Petrophysics, and Mechanistic Modeling groups. The team is currently refining logging and coring plans and determining the parameters of production test, including injection volumes, rates, and pressures. Work is proceeding on these tasks:
1) Pre-test evaluations of testing options including contingencies for low or no injectivity
2) Hydrate coring, core handling, and core testing
3) Well logging program

4) Nitrogen injection test design
5) Pressure transient test designs
6) CO_2 injection test design
7) Flowback test design

Well Design Team

The Well Design Team, also led by David Schoderbek, includes Anchorage-based ConocoPhillips personnel with expertise in regulatory affairs, drilling, completions, and testing. Current work being performed by the team includes:
1) Compilation of permitting and project timelines
2) Evaluation of well designs including vertical and directionally drilled
3) Review of completion design options
4) Development of rock strength estimates using shear and compressional sonic log data

Laboratory and Petrophysical Studies

Three laboratory and petrophysical studies supporting the production test were completed in the 2nd Quarter, 2009. The studies are summarized below. The full study reports are available as Appendices A, B, and C.

Appendix A: The Role of Free Water in Hydrate Reformation & Permeability
Author: James Howard, ConocoPhillips Company, Bartlesville, OK
The role of excess or free water in hydrate-bearing sediment that might alter the carbon dioxide exchange for methane was evaluated in a series of laboratory experiments. Previous laboratory experiments on the methane-carbon dioxide exchange were based on the assumption that all of the available initial water was converted into methane hydrate. Field evidence suggested that there may be some excess free water in the hydrate-bearing intervals. This observation raised concerns that injection of carbon dioxide would form carbon dioxide hydrate in the pore space that would reduce significantly the formation permeability.

Two experiments based on this design were completed. The first was a test of the concept while the second used higher initial and free water saturations to create an extreme case for permeability reduction. Initial hydrate formation was controlled by reducing the supply of methane to the water-saturated system and by adjustments of the pore pressure to values near the pressure-temperature stability for methane hydrate. The first test was run with a hydrate and free water saturation values each of 0.25 of the total pore volume, while the second test had hydrate and free water saturation values each of 0.35 of the total pore volume. The experimental results showed that the injection of carbon dioxide at reservoir conditions resulted in the rapid formation of additional hydrate in the pores. Despite this additional hydrate, permeability to gas was measured throughout the experiments. The inclusion of several depressurization steps at the conclusion of the second experiment provided some insights on the composition of the exchanged hydrate.

Appendix B: Predicting Methane Hydrate Saturation with the Stanford University Rock Physics Lab Code
Author: Robert Lankston, Geoscience Integrations, Missoula, MT)

This study compares hydrate saturations determined by applying code developed by the Stanford Rock Physics Lab with public saturation data from Mt. Elbert 1. Two other wells studied are NW Eileen St 2 and W Sak 24. One advantage of the Stanford code is it's ability to predict gas hydrate saturation with only two input parameters: acoustic impedance and resistivity ratio.

The Stanford Code predicts hydrate concentrations at Mt. Elbert 1 similar to those that have been reported by the BP-DOE team. The software was less successful at predicting saturations at the NW Eileen St 2 and W Sak 24 wells. Clipping of deep resistivity data and possible contamination of the sonic log data by dissociated gas may contribute to less than favorable results for these two wells. Graphical output of the Stanford code at W Sak 24 suggests free gas under the interpreted hydrate layer and water-saturated sandstone under the gas leg.

Where sonic logs are of questionable quality, the Stanford code is unable to accurately predict hydrate saturation. Many North Slope wells have poor quality sonic logs in the Gas Hydrate Stability Zone, and the need for a more robust prediction of gas hydrate stability led to a thorough investigation of hydrate petrophysics, described in the following study.

Appendix C: Petrophysical Evaluation of Potential Hydrate-Bearing Wells on the North Slope of Alaska

Author: Jason Mailloux, ConocoPhillips Company, Houston, TX

The primary goal of this project was to analyze the petrophysical response of common downhole logs to gas hydrates on the North Slope of Alaska and write a model to accurately determine the location and quantify the saturation of gas hydrate intervals. This study is complementary to investigation of the Stanford code, described in the previous section.

A model was developed to compare and evaluate four different methods: the NMR method, Archie's equation, the AIM solver module, and the Xu-White sonic method. This model was applied to 3 wells with known gas hydrate saturation as well as 17 wells that are candidate locations for the test well. Results show that this model is able to consistently predict saturation of hydrate bearing intervals.

Table 1 below summarizes results of the study. Of the 17 wells analyzed, W KUP 3-11-11 and L-106 are the wells with the strongest petrophysical evidence of hydrate occurrence. Both wells have downhole log responses similar to Mt. Elbert 1, NW Eileen St. 2, and Mallik 5L-38, all of which logged hydrate-bearing sandstones confirmed by coring.

Table 1 – Summary of Petrophysical Evaluation

Petrophysical Analysis of Hydrate Saturation		
Strong Indication	**Possible**	**Less Likely**
W Kup 3-11-11	1H-06	Kup St 7-11-12
L-106	NWE 1-01	Chev 18-11-12
	W Sak 24	3M-09
	NWE 2-01	

Cost Status

Expenses incurred during this quarter were below the Baseline Cost Plan as shown in Exhibit 1. The Baseline Cost Plan forecasted Federal expenses of $60,000 in the 2nd Quarter to secure long-lead items for the test. These commitments were not necessary during the 2nd Quarter, but may be incurred in the 3rd and/or 4th Quarters. The Non-Federal Incurred Cost was below Baseline Cost Plan due to fewer hours required by our Alaska and Technology staff to progress the project.

Exhibit 1 - Cost Plan/Status

COST PLAN/STATUS									
Project Phase ==>	**Phase 1, Site Ident.**		**Phase 2, Field Test Planning**			**Phase 3, Field Test**			
Baseline Reporting Quarter ==>	**Q408**	**Q109**	**Q209**	**Q309**	**Q409**	**Q110**	**Q210**	**Q310**	**Q410**
BASELINE COST PLAN									
Federal Share	0	0	60000	1450000	0	8315000	1300000	630000	0
Non-Federal Share	325100	499172	390875	333875	170699	361135	353410	348523	151351
Total Planned	325100	499172	450875	1783875	170699	8676135	1653410	978523	151351
Cumulative Baseline Cost	325100	824272	1275147	3059022	3229721	11905856	13559266	14537789	14689140
ACTUAL INCURRED COSTS									
Federal Share	0	0	0						
Non-Federal Share	121012	186099	275348						
Total Incurred Cost	121012	186099	275348						
Cumulative Incurred Cost	121012	307111	582459						
VARIANCE									
Federal Share	0	0	-60000						
Non-Federal Share	-204088	-313073	-115527						
Total Variance	-204088	-313073	-175527						
Cumulative Variance	-204088	-517161	-692688						

Milestone Status

The Milestone Status Report is shown in Exhibit 2 below.

Exhibit 2 – Milestone Status Report

MILESTONE STATUS REPORT						
#	Task/Subtask Description	Planned Start Date	Planned End Date	Actual Start Date	Actual End Date	Comments
	Field trial site selected	1-Oct-08	31-Mar-09	1-Oct-08	3-Apr-09	Top sites identified
	Partner negotiations completed	15-Feb-09	31-Mar-09	17-Mar-09		Ongoing
	Synergies with DOE-BP project identified	1-Mar-09	31-Mar-09	30-Mar-09		Ongoing
	Well test designed and planned	1-Apr-09	30-Sep-09	10-Mar-09		Underway
	Well and reservoir performance predicted	1-Jul-09	31-Dec-09			
	Field testing completed	1-Jan-10	31-Dec-10			
	Injection and production monitoring completed	1-Apr-10	30-Apr-10			
	Well abandonment complete	1-May-10	31-Dec-10			

Appendix A: The Role of Free Water in Hydrate Reformation & Permeability
Author: James Howard, ConocoPhillips Company, Bartlesville, OK

Introduction

An experiment was designed to investigate the effect on permeability when liquid carbon dioxide was injected in a hydrate-bearing interval that contained excess or free water. All of the previous laboratory experiments that have investigated the methane-carbon dioxide exchange were based on the assumption that all of the available initial water was converted into methane hydrate. Field evidence at Mt. Elbert suggests that there may be some excess free water in the hydrate-bearing intervals, which raises concerns that injection of carbon dioxide could result in formation of additional hydrate. Additional hydrate would reduce significantly the formation permeability.

Experiment

A Bentheim sandstone core plug was partially saturated with a 0.1 wt-percent NaCl brine (1,000 ppm NaCl or 0.018 Molar solution) by imbibition to a final water saturation of approximately 50%. The imbibition process generally leads to a uniform distribution of water along the length of the core as monitored by MRI techniques. Methane gas at 1200 psi was introduced to the core at one end of the core plug to fill the remaining pore space. The sample was then cooled to 4^{o}C, which initiated the formation of hydrate in the core as monitored by MRI (Figure A1). Previous experiments have allowed an unlimited amount of methane gas to the system in order to transform all of the available water to hydrate, but in this experiment, the methane volume was constrained so that roughly half of the available water was converted into hydrate. The comparison of methane consumption with the loss of MRI intensity as hydrate forms shows a general agreement, though it is noteworthy that the match is not as good as many previous experiments (Figure 1). This discrepancy will be examined more closely in the future.

Nitrogen gas was then used to flush any remaining methane from the spacers at the ends of the core plug. The nitrogen was connected to the outlet end of the core at 1200 psi and allowed to equilibrate for several days, during which MRI images were periodically collected at 19, 24, 28 and 40 hours after the nitrogen flush. The initial images showed no changes in hydrate saturation in the core, but after a period of 40 hours there was evidence of some dissociation at the outlet end of the core plug (Figure A2). The first image after 19 hours shows a rather inhomogeneous distribution of gas hydrate where the saturation of such is higher at the outlet of the core. Just before this scan, nitrogen was introduced to the system and was used to maintain pressure. No substantial MRI intensity changes occurred within the next 9 hours. At 32 hours, 1.5 pore volumes of nitrogen were injected as part of the permeability test. This exposed more of the methane hydrate to nitrogen, which resulted in the substantial dissociation observed at 40 hours.

Nitrogen was used in previous experiments to measure gas permeability in hydrate-bearing core samples, in part based on the assumption that small amounts of nitrogen would not disturb the methane-carbon dioxide hydrate equilibrium. It is clear from this

experiment and other recent tests in ConocoPhillips laboratories that while this assumption may be true for very small volumes of nitrogen that are used in simple permeability measurements, larger volumes of nitrogen raise the possibility of altering the hydrate equilibrium and causing limited dissociation.

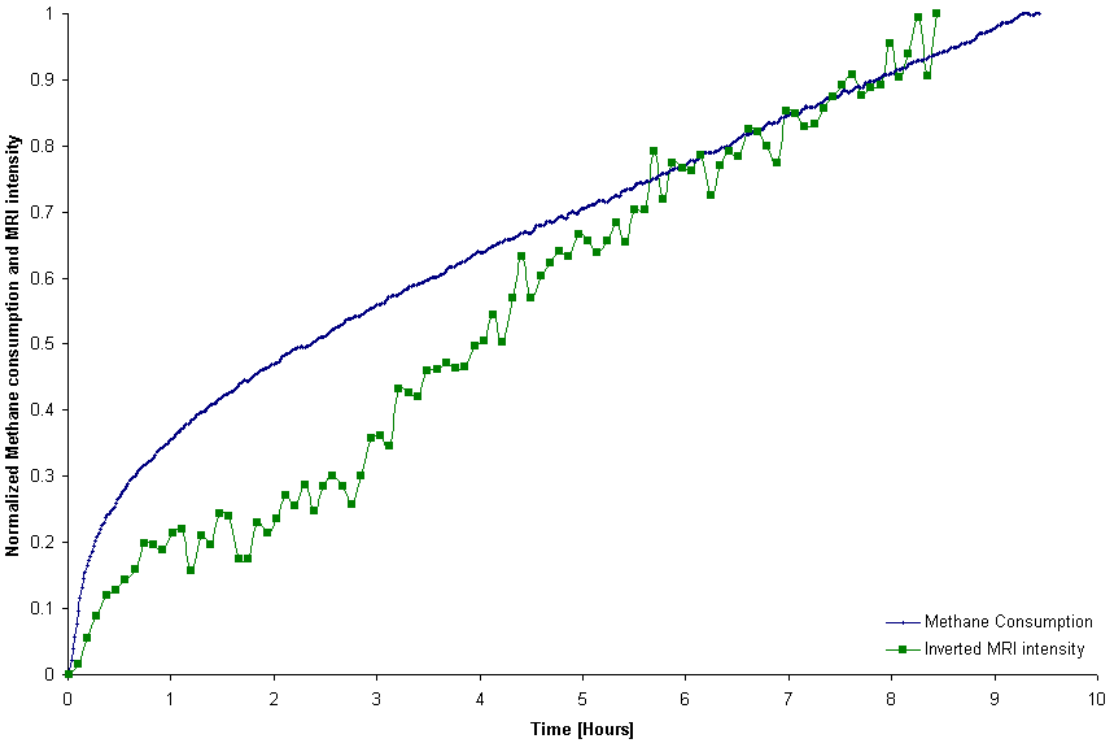

Figure A1. Methane consumption as measured in volume of gas during the formation of hydrate (blue) compared to the loss of MRI signal intensity during hydrate formation (green).

A series of rapid permeability measurements were made based on varying the rate of nitrogen injection and monitoring the differential pressure along the length of the core. Permeability values of 2 to 3 mD were determined on this sample in the presence of excess water. In this experiment the excess water and hydrate saturations were each at approximately 0.25 of the total pore volume, with free gas filling the remaining space.

Liquid carbon dioxide was injected into the hydrate-bearing core that contained slightly more excess water than initially designed because of the partial dissociation linked to the nitrogen injection. As expected, the carbon dioxide converted all of the available free water into a hydrate as monitored by the MRI (Figure A3). The saturation profile along the length of the core shows the somewhat uneven distribution of the initial water saturation (blue) and then the water saturation after methane hydrate formation and partial dissociation with the large volumes of injected nitrogen (red). There was significant noise in this intermediate image since the scan time was greatly reduced. The

final profile following the introduction of carbon dioxide showed the conversion of the remaining free water into hydrate (green).

Permeability was measured on the hydrate-bearing core after carbon dioxide converted the remaining free water into hydrate. Several short permeability tests run by injecting very small volumes of nitrogen gas returned values of 0.045 mD. After several tests the permeability was not measurable. Evidence from MRI images indicated that a hydrate plug formed in the inlet line of the core holder, thereby shutting down the continuous flow system.

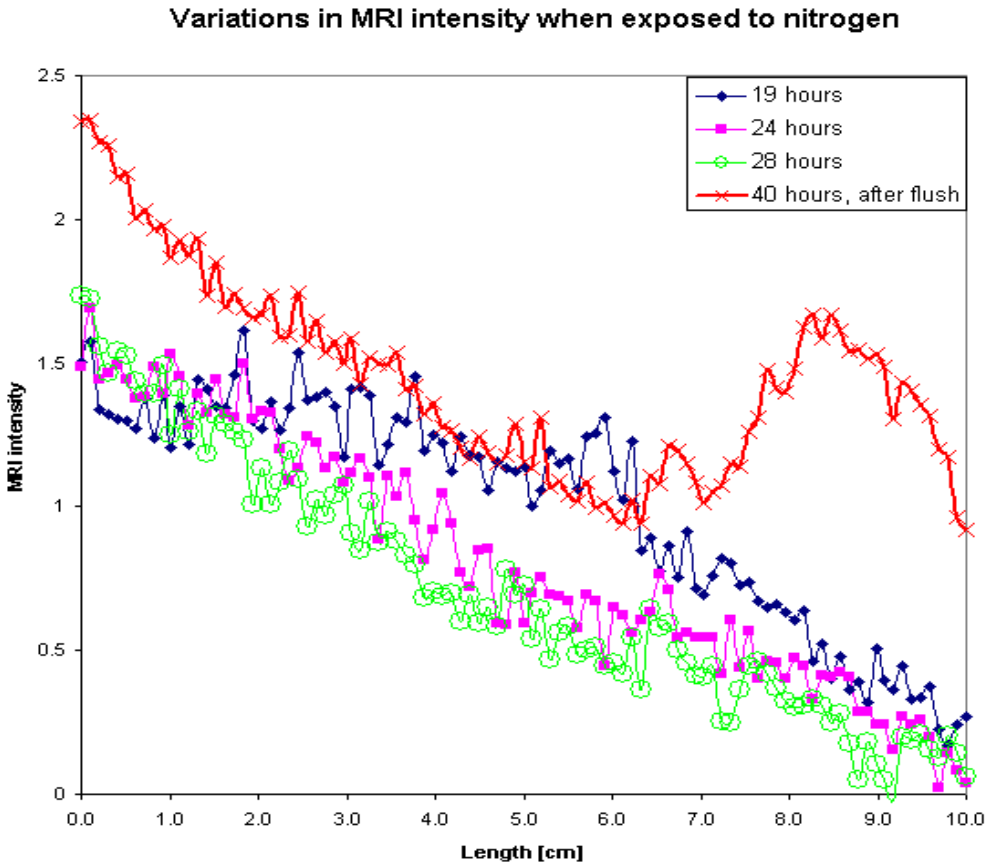

Figure A2. MRI intensity variations over the core length normalized by the average intensity from the image completed at 19 hours. A large nitrogen volume was injected just after the 28 hour scan.

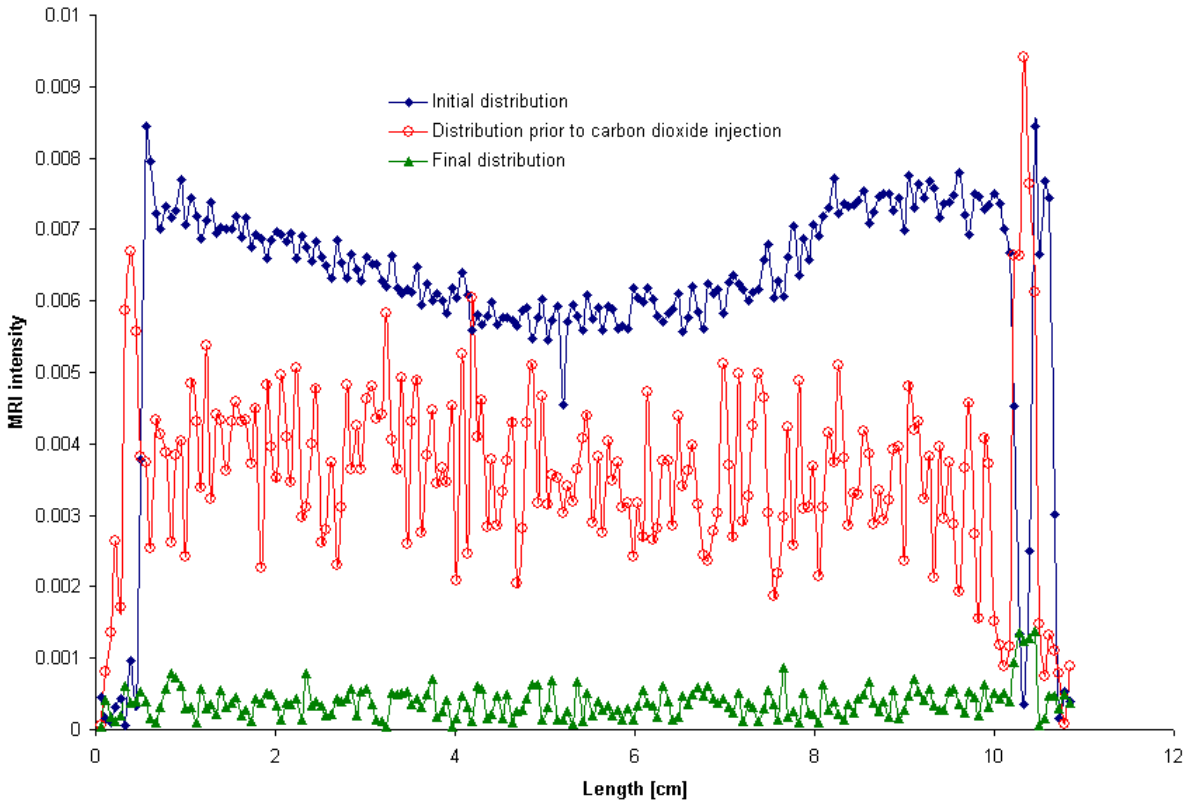

Figure A3. MRI generated profiles of water saturation along the length of the core at initial state (blue), following methane hydrate formation and prior to carbon dioxide injection (red) and following the formation of carbon dioxide hydrate (green).

Appendix B: Predicting Methane Hydrate Saturation with the Stanford University Rock Physics Lab Code

Author: Robert Lankston, Geoscience Integrations, Missoula, MT
Completed under the supervision of David Schoderbek, ConocoPhillips Upstream Technology

Executive Summary

The code developed by members of the Stanford Rock Physics Lab for predicting gas hydrate saturation was applied to log data from the Mt. Elbert, NW Eileen St 2, and W Sak 24 wells.

The software predicted hydrate concentrations at Mt. Elbert similar to those that have been reported by the BP-DOE team. The software was less successful at the NW Eileen St 2 site. Clipping of deep resistivity data and possible contamination of sonic log values by dissociated gas introduce unacceptable uncertainties in this approach.

Gas contamination may be a problem with W Sak 24 log data, also. The graphical output of the Stanford code suggests free gas under the interpreted hydrate layer and water-saturated sandstone under the gas leg.

Introduction

The Rock Physics Lab at Stanford University has an established program that provides insight into seismic responses caused by variations in rock and fluid properties in reservoirs. The lab has been involved with gas hydrates for at least ten years. In Gomez et al (2008) it is noted that, except for water saturations near 100%, the dependence of the elastic properties on hydrocarbon saturation is weak. As a result, quantifying water or hydrocarbon saturation is difficult because seismic velocity and impedance are controlled by the elastic properties of the mineral grains and the porosity of the rock. Porosity and water saturation together also impact resistivity measurements. Gomez et al (2008) presents a methodology to combine the velocity-impedance data and the resistivity data to determine saturations.

For this study, Stanford's Matlab code was exported to MicroSoft Excel Visual Basic for Applications and, the tests on Mt Elbert, NW Eileen State 2 and West Sak 24 described in the following sections were run in the Excel environment.

Methodology

The software generates a plotting canvas with axes of normalized resistivity (y) and P-wave impedance (x). The resistivity axis is logarithmic, and the impedance axis is linear (Figure B1). Upon this canvas a secondary mesh is generated that is used for estimating porosity and hydrocarbon saturation. Figure 1 shows the porosity-saturation mesh. The mesh is defined by gas gravity, pore fluid pressure, reservoir temperature, and brine salinity, which are parameters for the Batzle-Wang fluid density and modulus calculations. The gas hydrate module estimates the P-wave impedance given the density and modulus values from the Batzle-Wang module, values for porosity, saturation, and effective stress, and bulk modulus, shear modulus, and density values for quartz, clay, and gas hydrate.

The program assumes that the gas hydrate contributes to the solid component of the rock-fluid system and that the pore space not occupied by hydrate is filled with water. The code cannot currently accommodate water and free gas in the remaining pore space. Water filled pore space implies that the reservoir is below the base of permafrost.

In Figure 1, porosity is read along the more horizontal axis of the mesh. The values range from 0.15 at the right to 0.40 at the left. The mesh lines are spaced at intervals of 0.05. The more vertical axis in the mesh is water saturation. The grid lines vary from S_H of 0 at the bottom to S_H of 0.9 at the top of the mesh. The mesh extends only to $S_H = 0.9$ because at zero S_W, the resistivity ratio becomes infinite. High resistivity indicates high hydrate saturation.

The shape of the grid is consistent with rules of thumb derived from Collett (1993) where hydrate occurrence is indicated by resistivity values more than 50 times the background resistivity and sonic value 40 μs/ft less than the background transit time. The mesh provides some quantification of the hydrate saturation from the log responses.

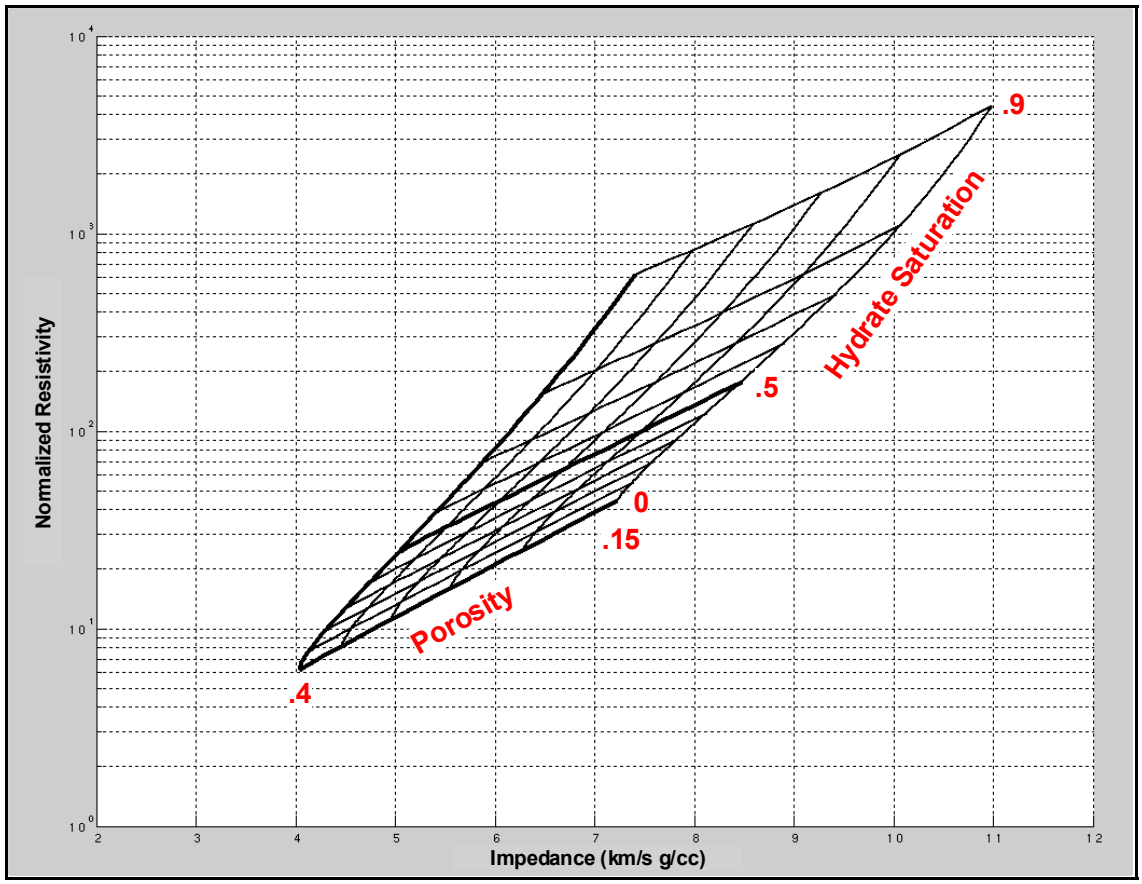

Figure B1: Basic Normalized Resistivity-P-wave Impedance Grid and Superimposed Porosity-Saturation Mesh**.** The vertical axis is the deep resistivity reading normalized by R_W. P-wave impedance is the product of P-wave velocity and bulk density.

Figure B2 shows the resistivity-impedance backdrop with the superimposed porosity-saturation mesh with a single data point at approximately 25% porosity and 70% hydrate saturation as read from the porosity-saturation mesh. The red dot in the example in Figure B2 is just one point. From well log data, a large number of points can be posted. Conceptually, points that post off the porosity-saturation mesh would be interpreted not to have met some criterion, most likely a shaley rock type instead of a sandy rock type. Another factor that could drive a point off of the mesh is a difference between the R_W value used in the calculation and the actual R_W in the reservoir. R_W uncertainty is addressed in a subsequent section.

Mt. Elbert Stratigraphic Test

The Mt. Elbert stratigraphic test was drilled during winter 2006-07 in the Milne Point Unit and the "C" & "D" sands of Collett (1993) were hydrate-bearing. Hydrate saturations from the "C" and "D" sands have been reported in the vicinity of 65% (Figure B3).

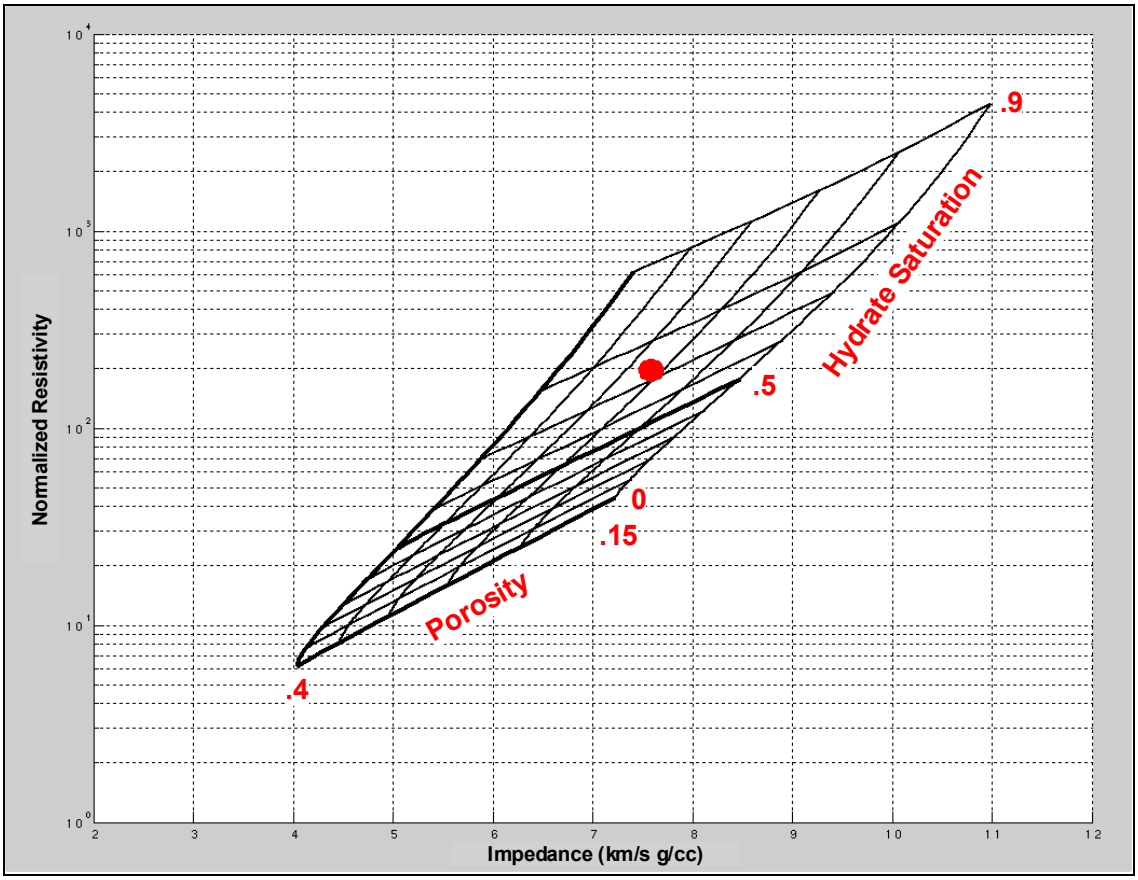

Figure B2: Analysis Template with a Sample Point. The red dot is posted on the normalized resistivity and impedance coordinate system. Its significance is read from the porosity-hydrate saturation mesh at (approximately) 25% porosity and 70% hydrate saturation. In the templates that follow, the saturation grid lines below 50% were eliminated.

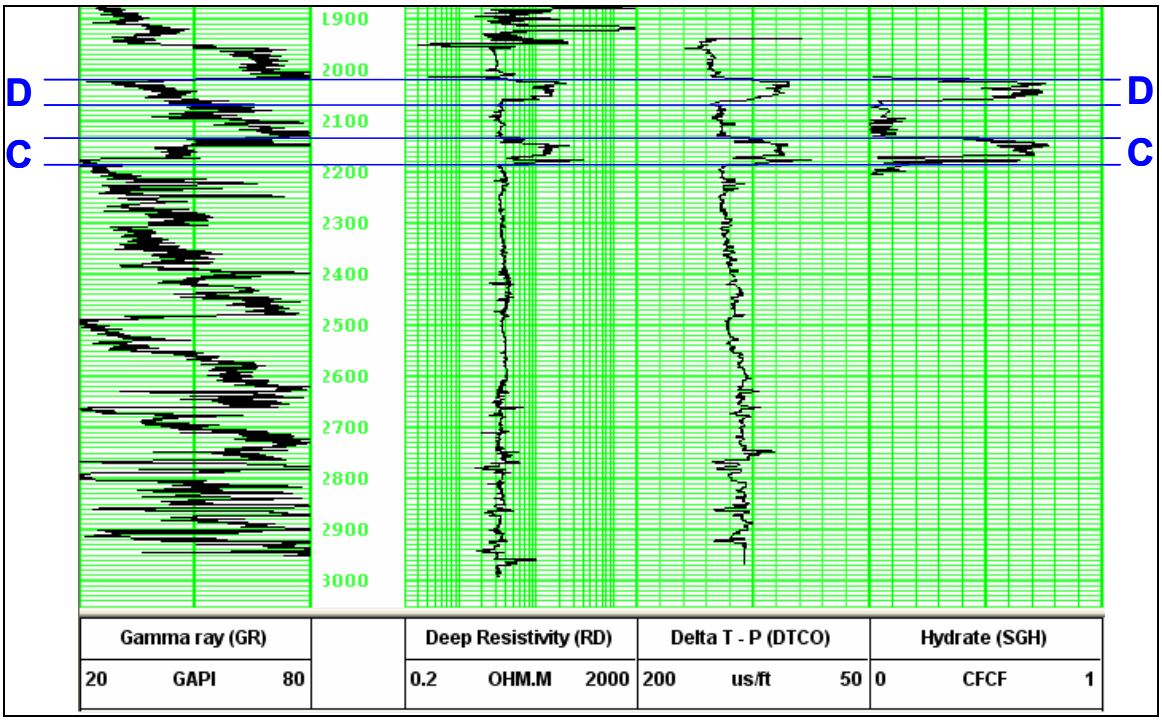

Figure B3: Logs from the Mt. Elbert Well. Sands "C" and "D" are indicated. Track 4 shows the estimated hydrate saturation in the two sands. The lower limit for the RD track is 2 ohm-m.

The template shown in Figure B4 for the Mt Elbert well was built with the following specifications:

Base of permafrost	1950 ft
Analysis depth	2030 ft
Temperature	33.2° F
Pressure	6.06 MPa
Humble constants	a = 0.62, m = 2.15
Gas specific gravity	0.6
Salinity	4900 ppm

Data Preparation

After the template is defined, the P-wave impedance and resistivity ratio values from the well log data must be calculated. Resistivity ratio is critically important and requires interpretive input; by contrast, P-wave impedance is simple to calculate.

Gomez et al (2008) define the resistivity ratio as R_T/R_W. Deep resistivity values are assumed to approximate R_T. R_W, however, is more elusive. R_{WA} has been estimated using a common equation,

$$\mathbf{R_{WA} = a\,\varphi^{m}}$$

where φ is porosity. For R_{WA} calculation in this study, porosity values from the density log have been utilized.

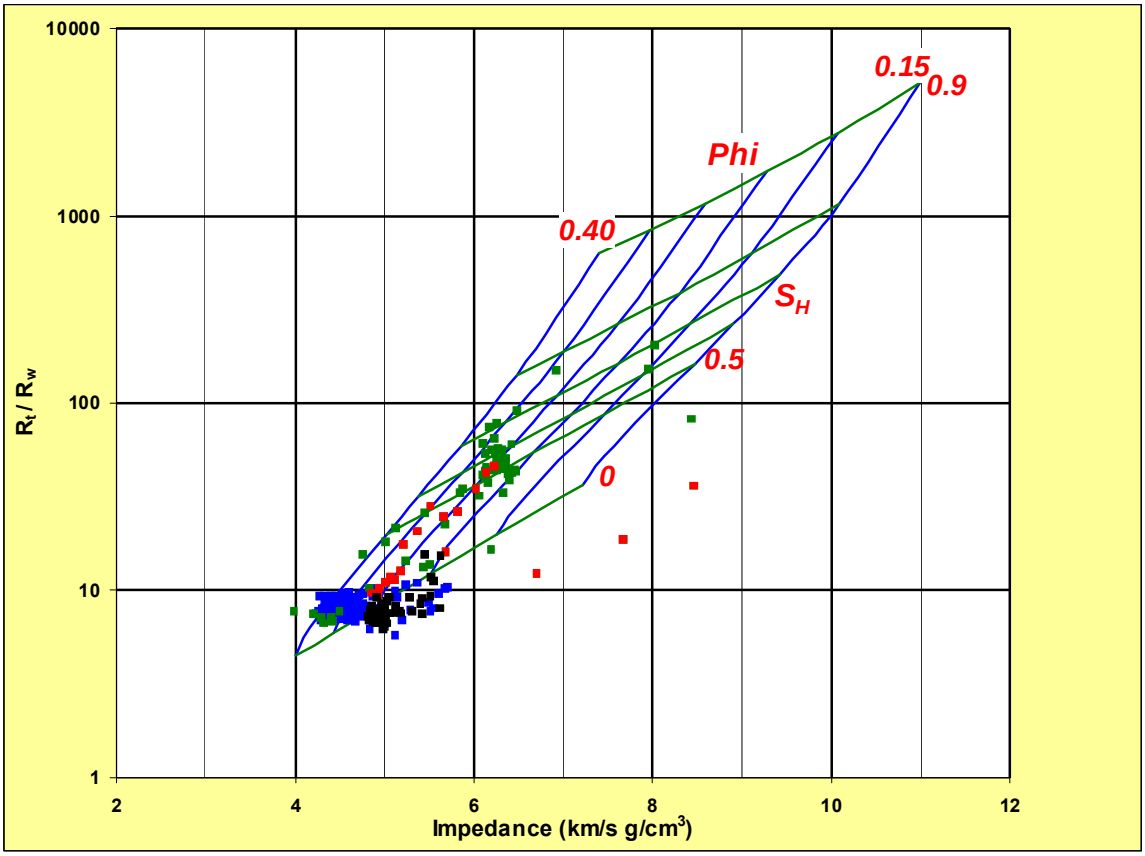

Figure B4: Analysis of Hydrate Concentration in the Mt. Elbert "C" Sand. Blue dots are from the water wet sand used to define R_{WA}. Black dots are from a shale section above the "C" sand. Green and red dots are from the "C" sand itself. The red dots are from the thin zone within the "C" sand that shows a marked decrease in resistivity and velocity.

The equation for R_{WA} presumes a 100% S_W condition. The "C" sand between 2190 ft. and 2280 ft. has a nearly constant resistivity response and appears to be water bearing. Similarly, the velocity log in this interval is consistent with a water nearing sand. Through this depth range the calculated R_{WA} is approximately 1. Entering a R_{WA}/salinity calculator with R_D = 11 ohm-m, porosity = 0.4, and formation temperature = 33.2° F, the resultant temperature-corrected R_{WA} = 1.2, which is used as the resistivity normalization factor for this well. The calculator also reports a salinity value of 4916 ppm equivalent NaCl. This was the basis for setting the salinity value for the template at 4900 ppm.

Results

Figure B4 shows three sets of color-coded points. The blue dots are from the water wet section used to estimate values for R_W, i.e., the depth range from 2190 to 2280 ft. The blue dots fall on the porosity-hydrate saturation mesh in the zone of porosity between 30 and 40% and in the S_W range of 85 to 100%. These values are consistent with the porosities observed on the density porosity log and with the interpretation of 100% S_W from the resistivity and velocity logs.

The set of black dots is drawn from the depth range of 2100 to 2135 ft, which is a shaley zone above the interpreted hydrate-bearing "C" sand. The black dots fall mostly outside of the analysis mesh, which is expected, given that they constitute the "wrong" lithology.

The last set of points is displayed in green and red. These dots are drawn from the "C" sand, i.e., 2140 to 2190 ft. Qualitative analysis of the resistivity and velocity logs indicates that this sand is hydrate-bearing. This is the zone, therefore, on which to test the utility of the analysis mesh. While the green dots show scatter, they cluster along the porosity grid line at 30% and in the hydrate saturation range of 50 to 60%. This is consistent with the 65% hydrate saturation reported from the Mt. Elbert well (Figure B3).

Figure B5 is the analysis graph for sand "D". The blue dots in this case can be considered a blind test of the method. This set of points is drawn from the depth range of the "B" sand, i.e., 2480 to 2550 ft. The blue dots indicate nearly 100% S_W and porosities in the 30 to 40% range, generally consistent with open hole porosity logs. The red dots in Figure B5 are from sand "D." Many of the points form a cluster with a center at porosity = 35% and hydrate saturation of 60%. Another cluster is centered near the same porosity but at S_H about 50%. Both clusters appear consistent with the S_H track in Figure B3.

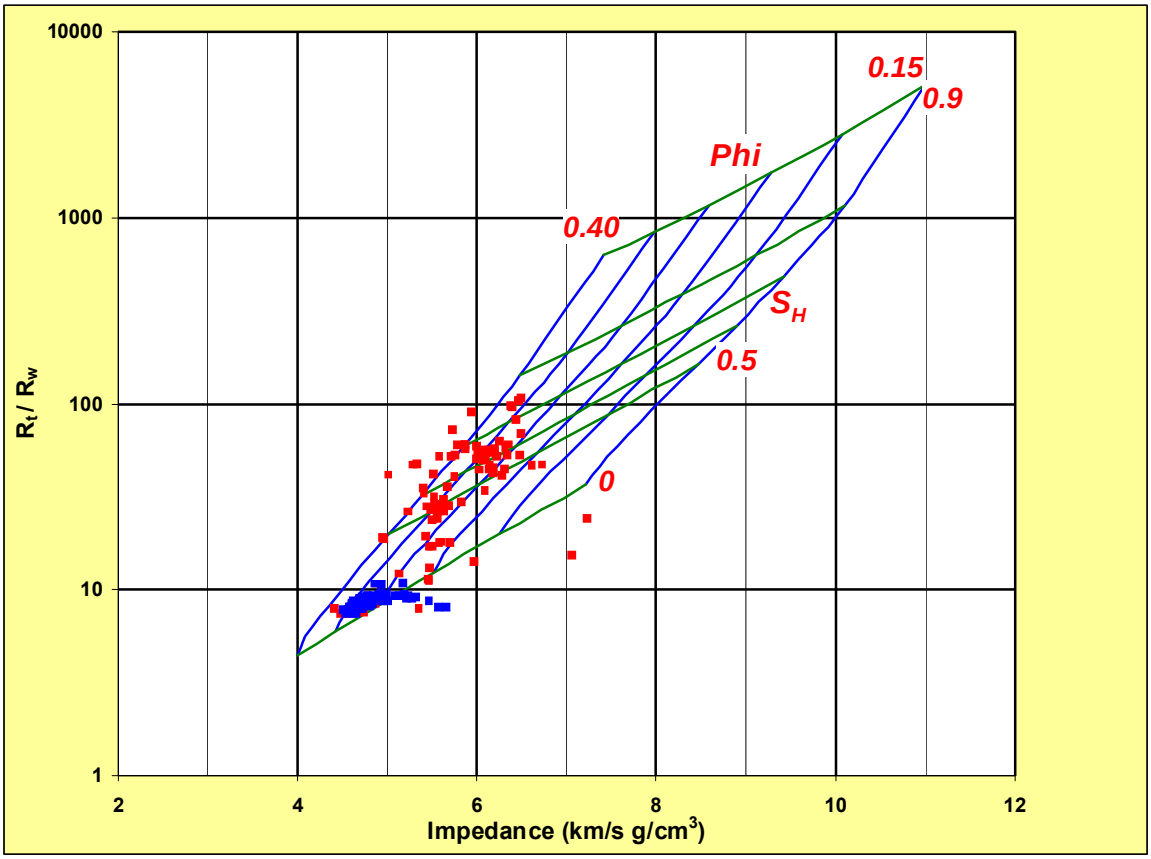

Figure B5: Analysis of the Mt. Elbert "D" Sand. Blue dots are from the B sand, which is interpreted to be water saturated. Red dots are from the sand "D." One cluster of "D" sand points is centered at porosity = 35% and hydrate saturation of 60%, which is consistent with the hydrate concentration track in Figure 3.

Figure B6 shows the results of plotting the values from sand "B" and sand "D." The sand "B" points (blue in Figure B6) serve as control on the process and parameter specifications. The cluster of approximately 120 points from sand "B" (blue) indicate nearly 100% water saturation and porosities in the 30 to 40% range. The porosities generally agree with the density porosity values in the log display (Figure B1-2).

Most of the red dots in Figure B6 fall off of the porosity-hydrate saturation mesh, i.e., the impedance values seem to be too low. If the section contains gas, both the P-wave velocity and the density will be suppressed, and impedance values will be shifted to lower values, i.e., to the left off of the range of the mesh in Figure B6.

If this interpretation is correct, it illustrates a potential complication in using this method for estimating gas hydrate concentration from the wireline logs. Gas in the system may be a result of hydrate dissociation during the time between penetration of the reservoir by the drill bit and logging. The effect of gas in the system moves the impedance coordinate to the left, i.e. to lower values. Deep resistivity value should be minimally affected by the free gas in the near-wellbore pores. Shifting the dots to the right, onto the mesh, until they are coincident with porosity values measured on the density log, is a logical work-around to obtain the approximate range of saturations. After making such a shift in

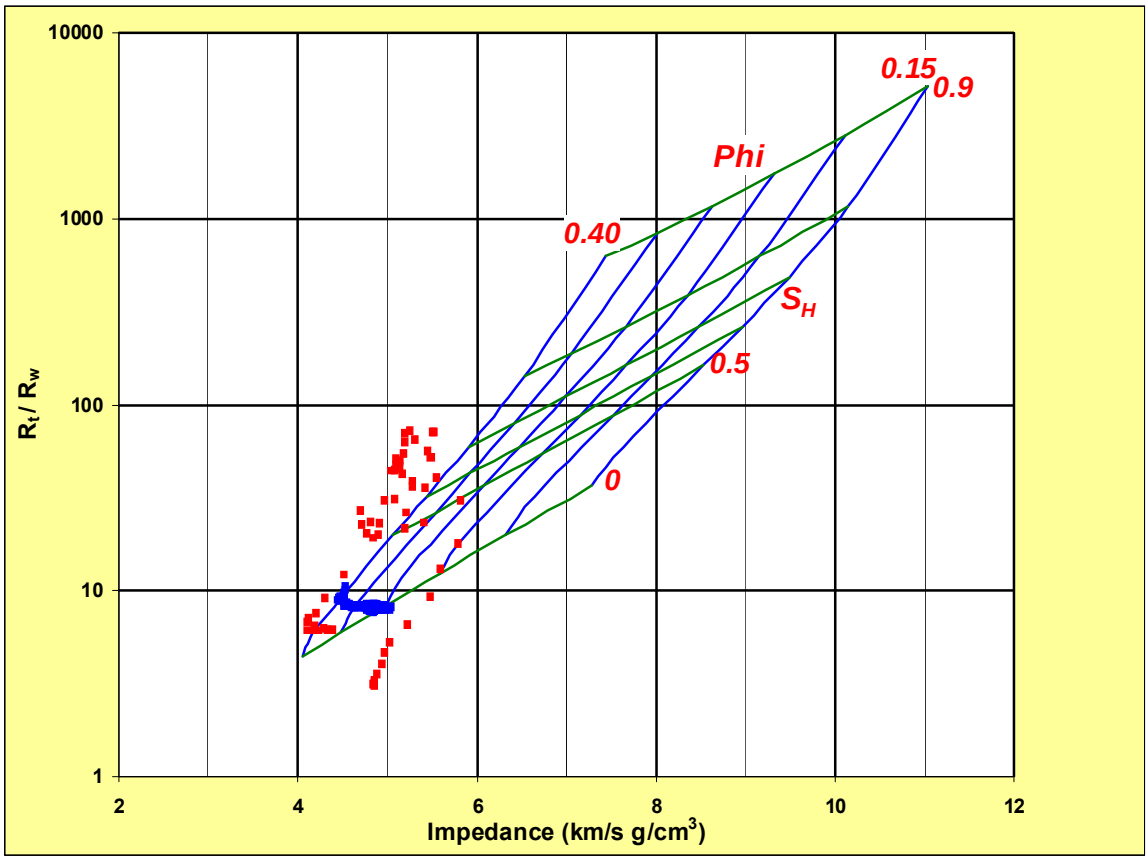

Figure B6: Analysis of the NW Eileen St 2 "B" and "D" Sands. The blue dots are from the "B" sand, which is interpreted to be water saturated in this analysis. The red dots are from the "D" sand. The dots fall off of the mesh because of gas in the reservoir.

Figure B6 for the "D" sand, the hydrate saturation is estimated in the range of 50 to 70%.

The "C" sand at NW Eileen St 2 introduces another complication to the analysis (Figure B7). Resistivity values on the wireline log for the "C" sand appear to be clipped at 2000 ohm-m. Dividing 2000 ohm-m by the R_{WA} value of 4 ohm-m yields a resistivity ratio of 500. A line of dots is posted at the 500 level in Figure B7. A notable cluster of these points, like the points for sand "D" (Figure B6), is off the left side of the porosity-saturation mesh. As in the case of sand "D," the impedance values probably require shifting some amount to the right, and the resistivity ratio values should be shifted by some unknown amount in the vertical sense to account for the clipping. Pre-drill hydrate concentrations in excess of 90% may have been present in the "C" sand.

Thus log quality and the presences of gas in the hydrate pore space both introduce

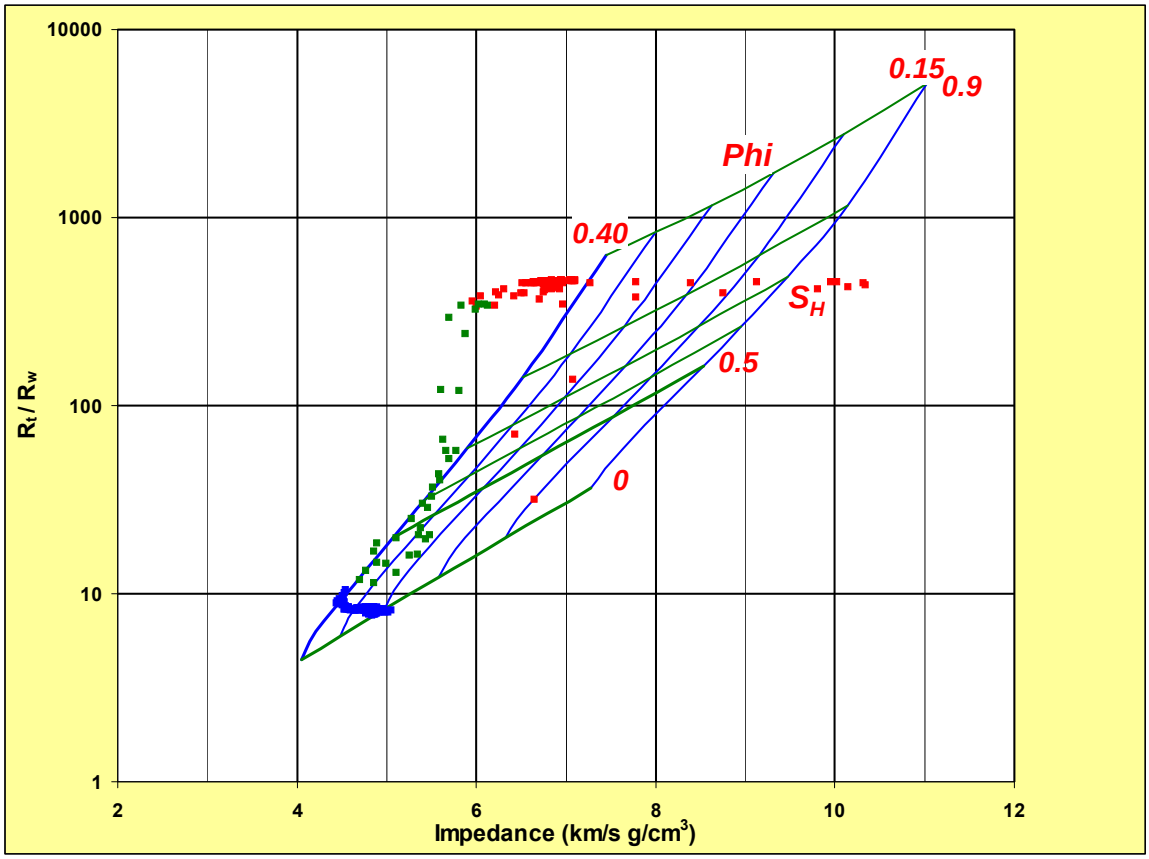

Figure B7: Analysis of the NW Eileen St 2 "B," "C," and "E" Sands. The blue dots are from the water saturated "B" sand, as in Figure 6. The red dots are from the "C" sand, and the green dots are from the "E" sand. The "C" and "E" points appear to underestimate the porosity, as discussed in the text. Many of the "C" points are posted at too low a resistivity ratio value because of clipped log values.

significant uncertainties in the saturations calculated by this method.

West Sak 24

Figure B8 is the analysis graph for the "B" sand at W Sak 24. Three sets of points are plotted. The red dots are from the interpreted hydrate-bearing section. As was the case with sand "C" at NW Eileen St 2, the resistivity values had been clipped to 2000 ohm-m, leading to a resistivity ratio that is too low. In addition, as with the NW Eileen St 2 sands, the hydrate-bearing sand points (red) appear to show the influence of free gas because the impedance is too low. Therefore, no quantitative estimate of the hydrate concentration can be made.

If the section below the hydrates is gas-bearing, then the points from this interval should not plot on the porosity-hydrate saturation mesh, as can be seen in Figure B8. The black dots all plot to the left of the mesh. The low impedance values are consistent with gas in the fluid phase.

Finally, if the lowest section is water saturated, the resistivity ratio-impedance points

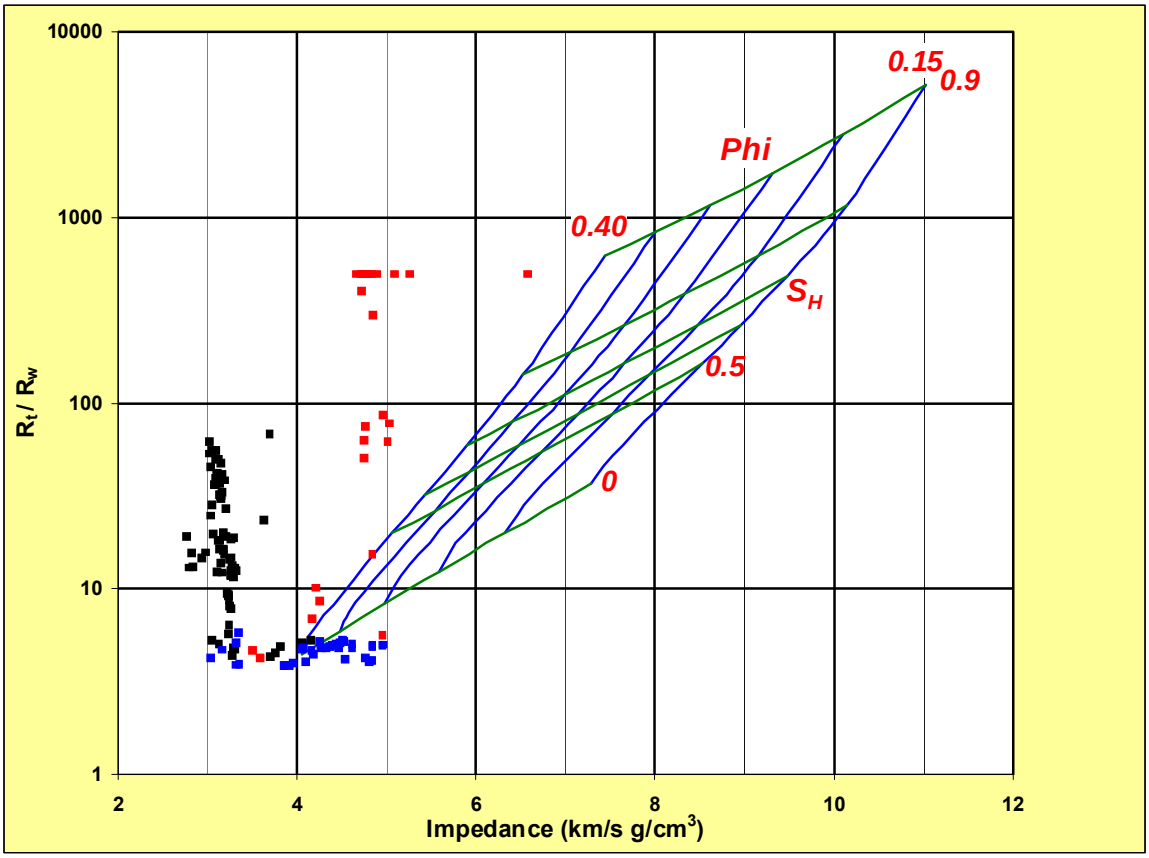

Figure B8: Sand "B" from W Sak 24. The red dots are from 13 ft of section at the top of the "B" sand. The resistivity values were clipped at 2000, and they show the influence of gas perhaps from hydrate dissociation. The black dots are from 36 ft of section immediately below the upper, possibly hydrate-bearing section. The lower section can be interpreted to be gas-bearing. The blue dots are from 18 ft below the gas leg and can be interpreted as a water-saturated section.

should plot at the bottom of the porosity-hydrate saturation mesh, as can be seen in Figure B8. This observation not only strengthens the qualitative interpretation of the log responses, but it also provides some validation for the decision to maintain the R_W value at 4 ohm-m, which is the same value that used for the NW Eileen St 2 analysis.

Summary

The code that was developed at the Stanford University Rock Physics Lab (Gomez et al, 2008) returns viable estimates of gas hydrate saturation where high quality well logs are available. Application of the code to the data from the Mt. Elbert well has yielded hydrate estimates consistent with those published by the Mt. Elbert team.

Application of the code to the data from the NW Eileen St 2 well identified two concerns. The first is that the very high resistivity values in the "C" sand are clipped to 2000 ohm-m. This precludes calculation of an accurate resistivity ratio. The second is that the calculated impedance values appear too low, since the plotted points do not fall on the porosity-hydrate saturation mesh. This is interpreted to indicate either that gas was present in the hydrate pore space prior to drilling or that hydrate dissociated prior to logging.

Finally, the Stanford code was applied to the data from the W Sak 24 well, The analysis indicates the presence of a 13 ft thick hydrate-bearing zone at the top of the "B" sand. Unfortunately, the sonic values appear to be contaminated by gas. The hydrate-bearing sand appears to overlie a gas-bearing section of the "B" sand, and data from that log interval plots off of the mesh, as expected. Finally, a water-saturated interval underlies the gas-bearing section. Computed data points from this section plot along the 100% S_W line in the mesh.

References

Collett, T.S., 1993, Natural gas hydrates of the Prudhoe Bay and Kuparuk River area, North Slope, Alaska: *AAPG Bulletin*, American Association of Petroleum Geologists, v. 77, no. 5, p 793-812

Collett, T.S., W.F. Agena, M.W. Lee, M.V. Zyrianova, K.J. Bird, R.R. Charpentier, T. Cook, D.W. Houseknecht, T.R. Klett, R.M. Pollastro, C.J. Schenk, 2008, Assessment of Gas hydrate Resources on the North Slope, Alaska, 2008: USGS Fact Sheet 2008-3073, 4pp

Gomez, C.T., J. Dvorkin, and G. Mavko, 2008, Estimating the hydrocarbon volume from elastic and resistivity data: A concept: *The Leading Edge*, Society of Exploration Geophysicists, June 2008, p 710-718

Appendix B-A

Logs for Mt. Elbert, NW Eileen St 2, and W Sak 24

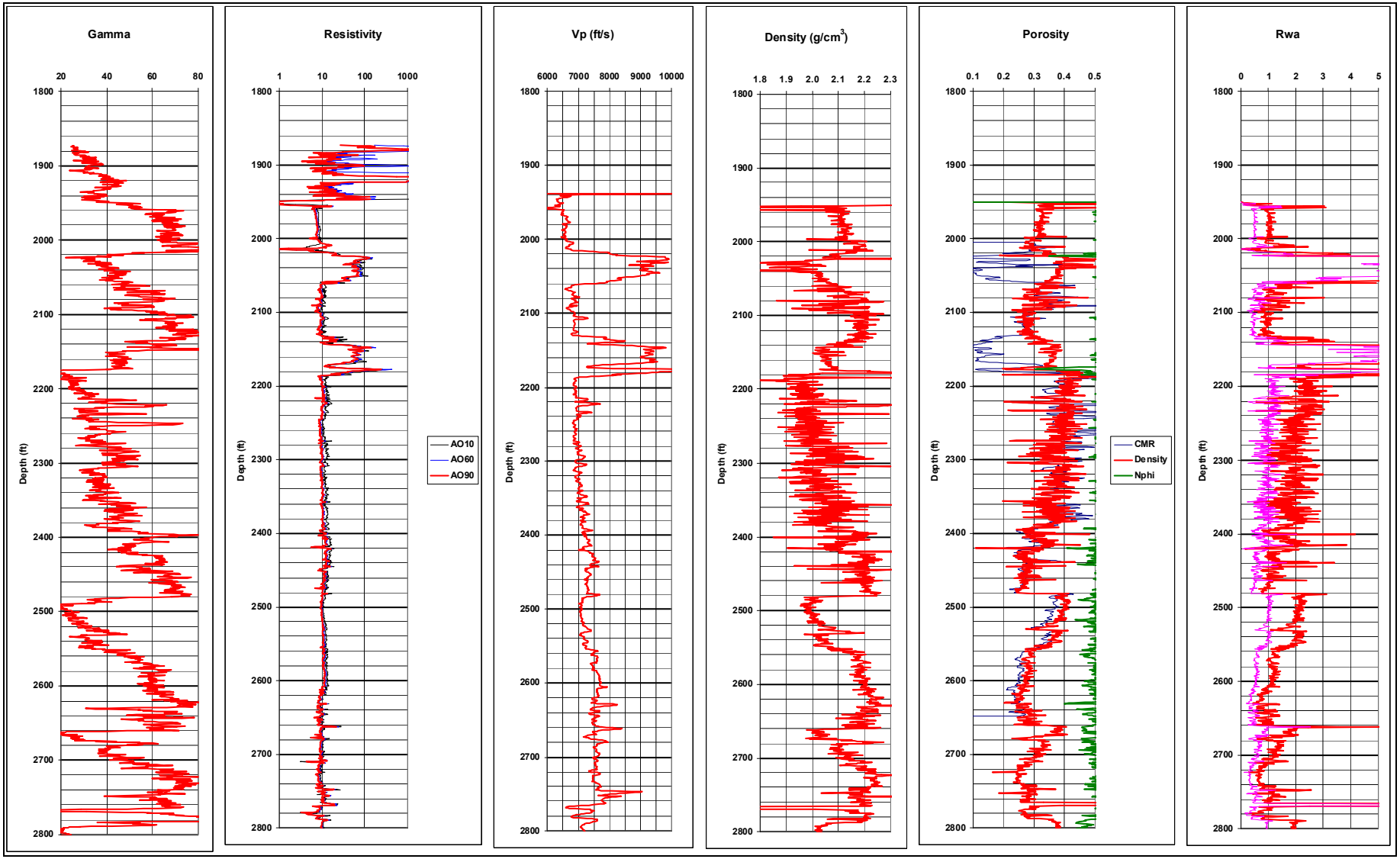

Figure B-A-1: Logs from Mt. Elbert #1 well: The pink curve in the R_{wa} track is the temperature corrected value. The temperature was set to temperature in the C sand, i.e., 33.2^{o} F.

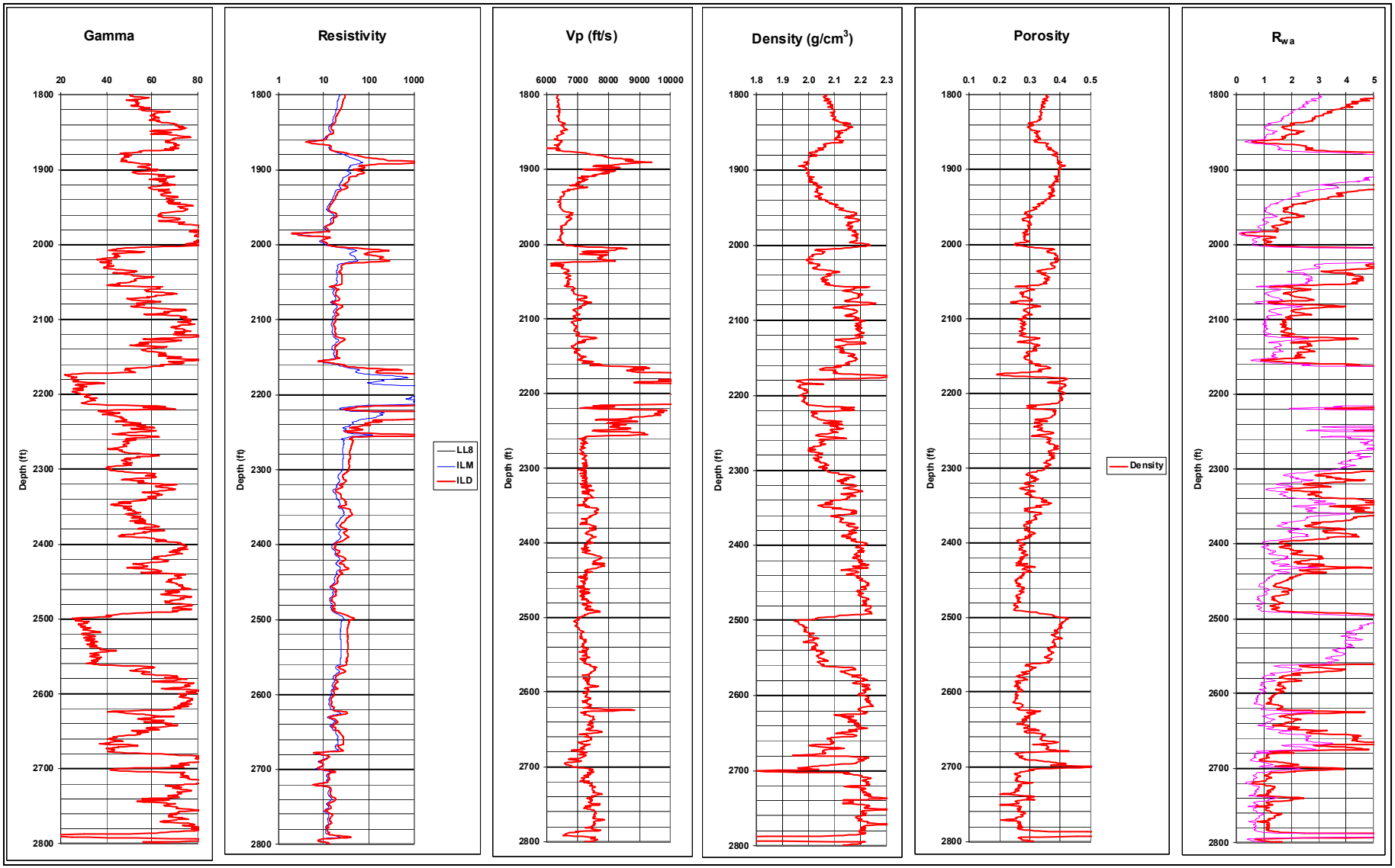

Figure B-A-1: Logs from NW Eileen St #2 well: The pink curve in the R_{WA} track is the temperature corrected value based on the temperature in the B sand.

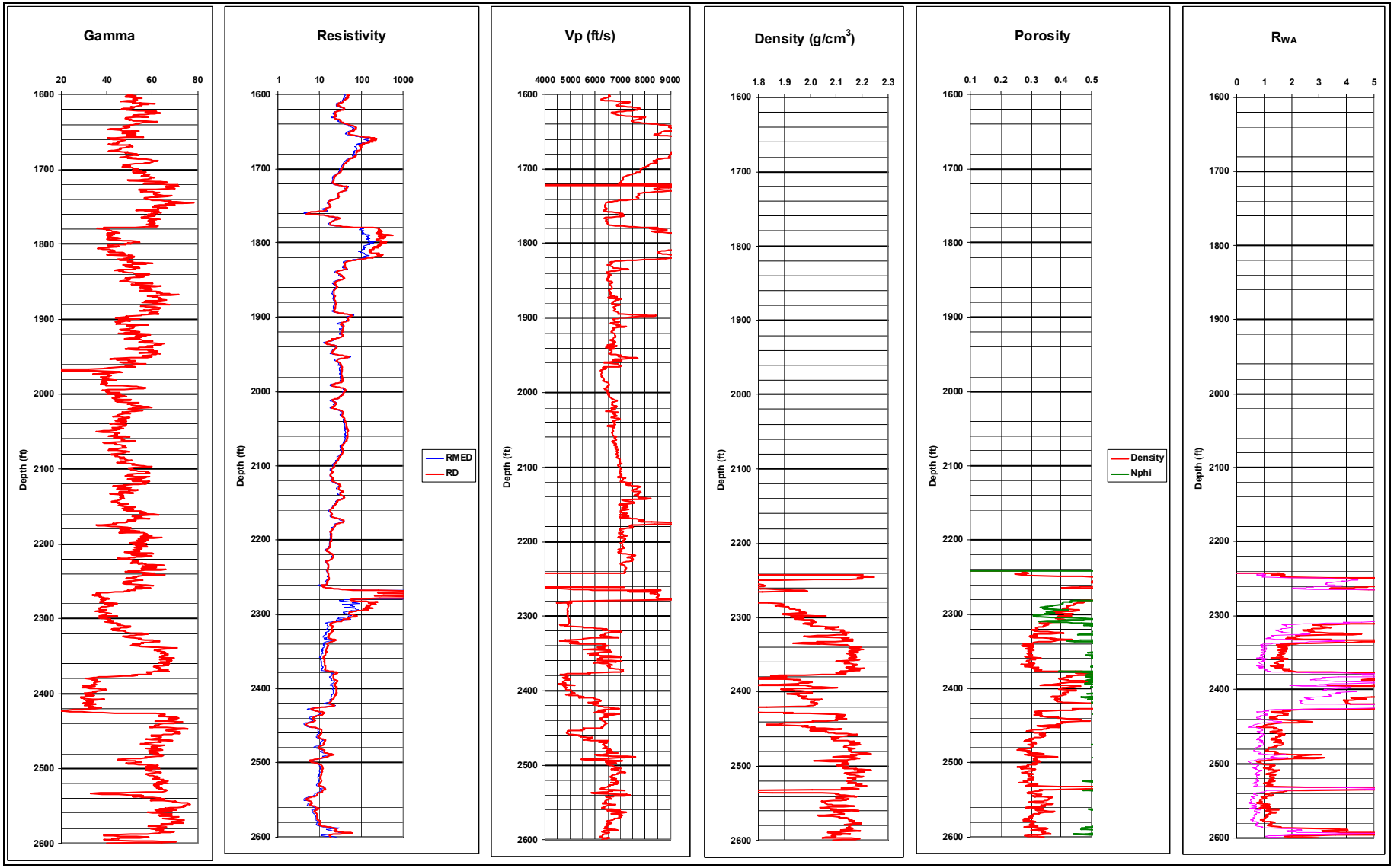

Figure B-A-2: Logs from W Sak #24 well: The pink curve in the R_{WA} track is the temperature corrected value based on the temperature in the B sand.

Appendix C: Petrophysical Evaluation of Potential Hydrate-Bearing Wells on the North Slope of Alaska

Author: Jason Mailloux, ConocoPhillips Company, Houston, TX
Completed under the supervision of David Schoderbek & Jim Klein, ConocoPhillips Upstream Technology

Executive Summary

The properties of gas hydrates have been studied by many workers over the past 20 years, but this work has not yet led to the exploitation of a resource that has been estimated to have more than twice the energy of all known coal, oil and gas. In recent years, studies have been conducted examining a thermodynamically favorable CO_2-methane exchange in gas hydrates that does not dissociate the hydrate. To select a location to test this method in the field, the characteristics of natural gas hydrates need to be calibrated to their log response. To meet this need, a module was developed in Geolog to accurately determine hydrate saturation using common downhole logs by four different methods: the NMR method, Archie's equation, the AIM solver module, and the Xu-White sonic method. This module was applied to 3 wells that are known to contain gas hydrate as well as 17 wells that are considered to be potential locations for the test well. Results show that this module is able to characterize hydrate bearing intervals.

Objective:

The primary goal of this project is the study of petrophysical response of common downhole logs to gas hydrates on the North Slope of Alaska and generation of a program within Geolog to accurately identify hydrate occurrence and quantify gas hydrate saturation in gas hydrate-bearing intervals. The findings of this study will be used to aid in determination of the best location for the aforementioned test well. The modules will also be used to assist in the evaluation of the test well.

Petrophysical response of gas hydrate:

Collett and Ladd (2000) presented the following summary (1-6) of the responses of common downhole logs based on data from a confirmed gas hydrate interval in Northwest Eileen State 2. Item 7 is an addendum to their list:

1. Electrical Resistivity (Dual Induction) log: there is a relatively high electrical resistivity deflection on this log in a gas hydrate zone, compared to that in a water saturated horizon.
2. Spontaneous Potential (SP) log: there is a relatively lower (less negative) spontaneous-potential deflection in a gas hydrate–bearing zone when compared to that associated with a free-gas zone.
3. Caliper log: the caliper log in a hydrate usually indicates an oversized borehole resulting from spalling associated with gas-hydrate decomposition.
4. Acoustic Transit-Time log: within a gas hydrate there is a decrease in acoustic transit time in comparison to a unit saturated with either water or free gas.
5. Neutron Porosity log: in a gas hydrate there is a slight increase in the neutron porosity; this response contrasts with the apparent reduction in neutron porosity in a free-gas zone.
6. Density (Porosity) log: within a gas hydrate there is a slight decrease in density compared to a unit saturated with water.

7. Magnetic Resonance Porosity log: A significant decrease in magnetic resonance porosity (referred to by the generic acronym NMR and the Schlumberger acronyms CMR and TCMR) is noted in known hydrate-bearing zones.

The two most frequently observed responses in known hydrate-bearing intervals are a large increase in the electrical resistivity and a large decrease in acoustic transit time (Figures C1 and C2). From a petrophysical perspective, hydrates are viewed as a part of the rock matrix because they are solid and support a shear wave, a property not shared with free natural gas, oil, or water. Being a solid, they are "faster" than gas or water because sound waves propagate more quickly through a solid than through a fluid, resulting in a decrease in acoustic transit time. The neutron porosity, density, spontaneous potential and caliper responses are too slight to be diagnostic of gas hydrate without the electrical resistivity and acoustic travel time logs. Magnetic resonance logs have been run in very few North Slope wells drilled through hydrate-bearing sections, so robust technique to determine hydrate saturation from commonly available logs has been devised.

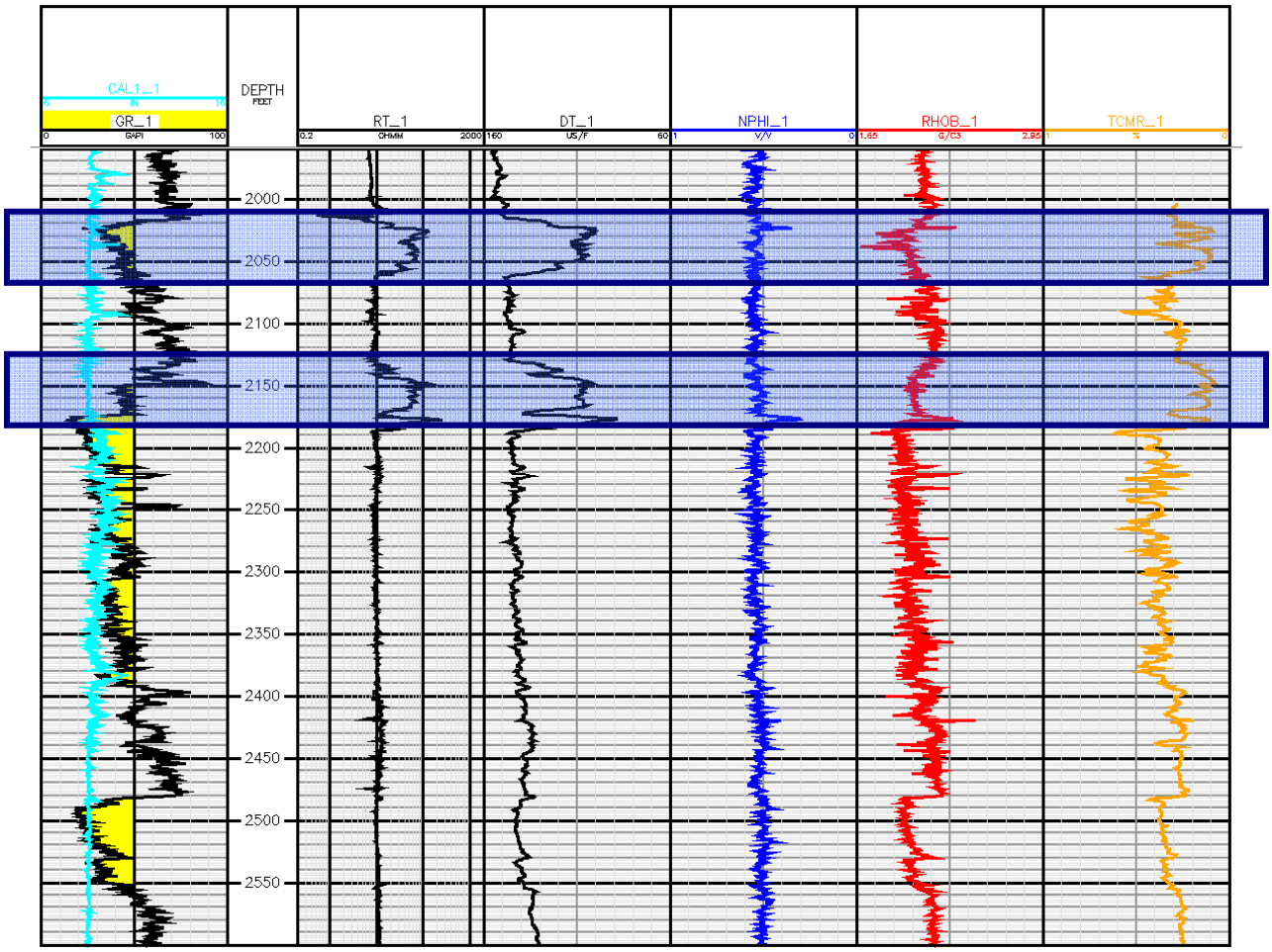

Figure C1. Mt Elbert well logs that illustrate the typical downhole log responses to gas hydrates as outlined by Collett and Ladd (2000). Known hydrate intervals are highlighted in blue. There are significant responses from the sonic, resistivity and TCMR logs, but little to no response in the other logs. The SP log was not available for this well.

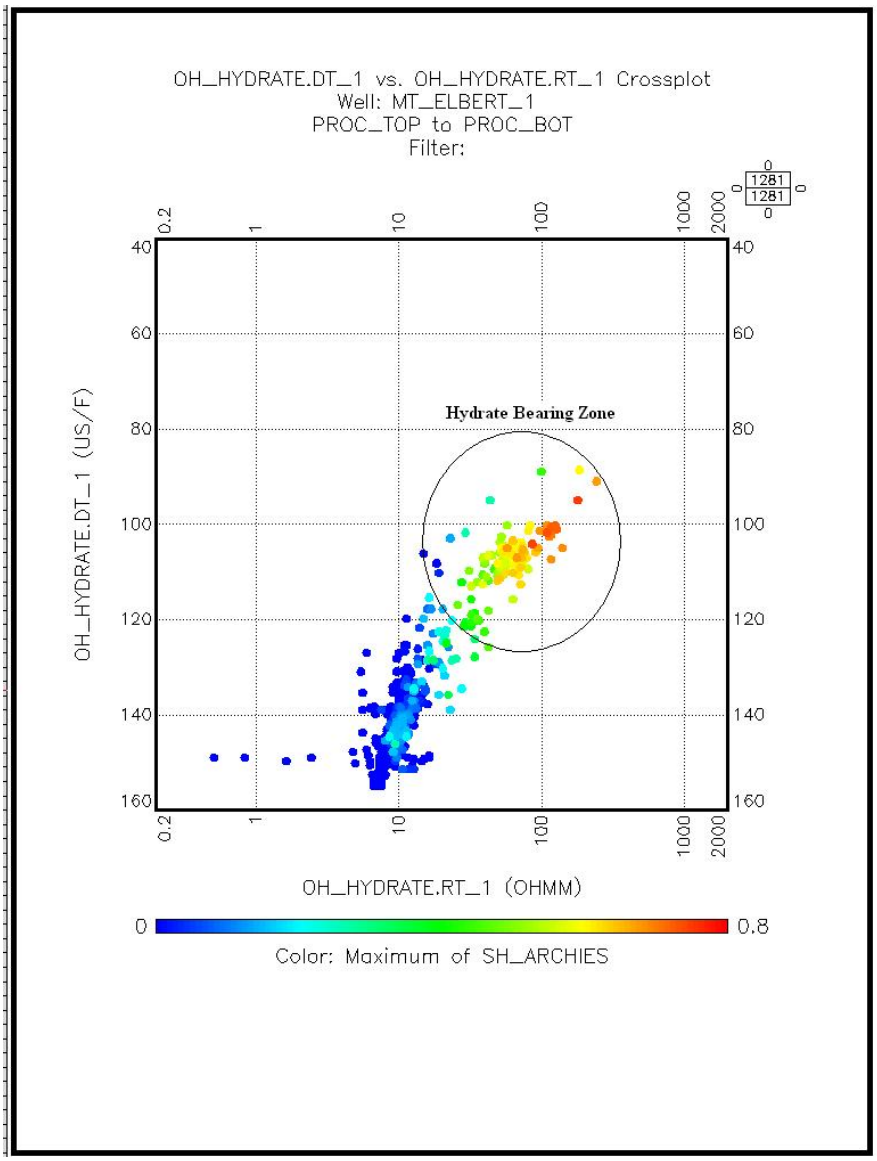

Figure C2. Resistivity versus sonic cross plot for Mt. Elbert well (data points colored by hydrate saturation, calculated using Archie's equation). High electrical resistivity and high acoustic velocities are typical of gas hydrates.

Models for identifying and quantifying hydrate saturation:
There are multiple models for identification of hydrate-bearing strata and estimating gas hydrate saturation. They group into the following four categories:

1. Magnetic resonance method
2. Archie's equation
3. Simultaneous equation solvers
4. Sonic methods

Magnetic Resonance Method

Kleinberg et al. (2005) used NMR to determine hydrate saturation. This method requires only the CMR porosity and density logs to make an accurate estimate of hydrate saturation. Density porosity must first be calculated to use the NMR method (Equation 1). This method is based on the fact that magnetic resonance porosity is much less than density porosity in hydrate zones because the hydrate is not detected by NMR, thus hydrate saturation is calculated using the difference between the two logs (shown in Equation 2).

1. $$DPHI = \frac{\rho_{matrix} - \rho_{bulk}}{\rho_{matrix} - \rho_{fluid}}$$

2. $$S_h = \frac{DPHI - TCMR}{DPHI + \lambda \cdot TCMR}$$

3. $$\lambda = \frac{\rho_{fluid} - \rho_{hydrate}}{\rho_{matrix} - \rho_{fluid}}$$

The biggest advantage to this method is that there are no well-specific parameters such as R_w or pore aspect ratio and bulk and shear moduli in the sonic method, all of which can be difficult to determine a priori. The NMR method requires only fluid, matrix, and hydrate densities, which are essentially constants.

Archie's Equation

There are several papers that have used some form of Archie's equation (1942) to determine hydrate saturation (Collett, 1998; Collett and Ladd, 2000; Collett; 2001, Miyairi et al., 1999, and others). Collett (1998) chose to use so-called "Humble" values for *a* (0.62), *m* (2.15), and *n* (1.93). Archie constants which are considered applicable for granular matrix systems. The Humble parameters did not work well for the wells analyzed in this study. Standard Archie constants (*a*=1, *m*=2, *n*=2) fit best the porous strata evaluated in this study. Figure C3 illustrates a Pickett plot from the Mt. Elbert hydrate well using the standard values for Archie's constants.

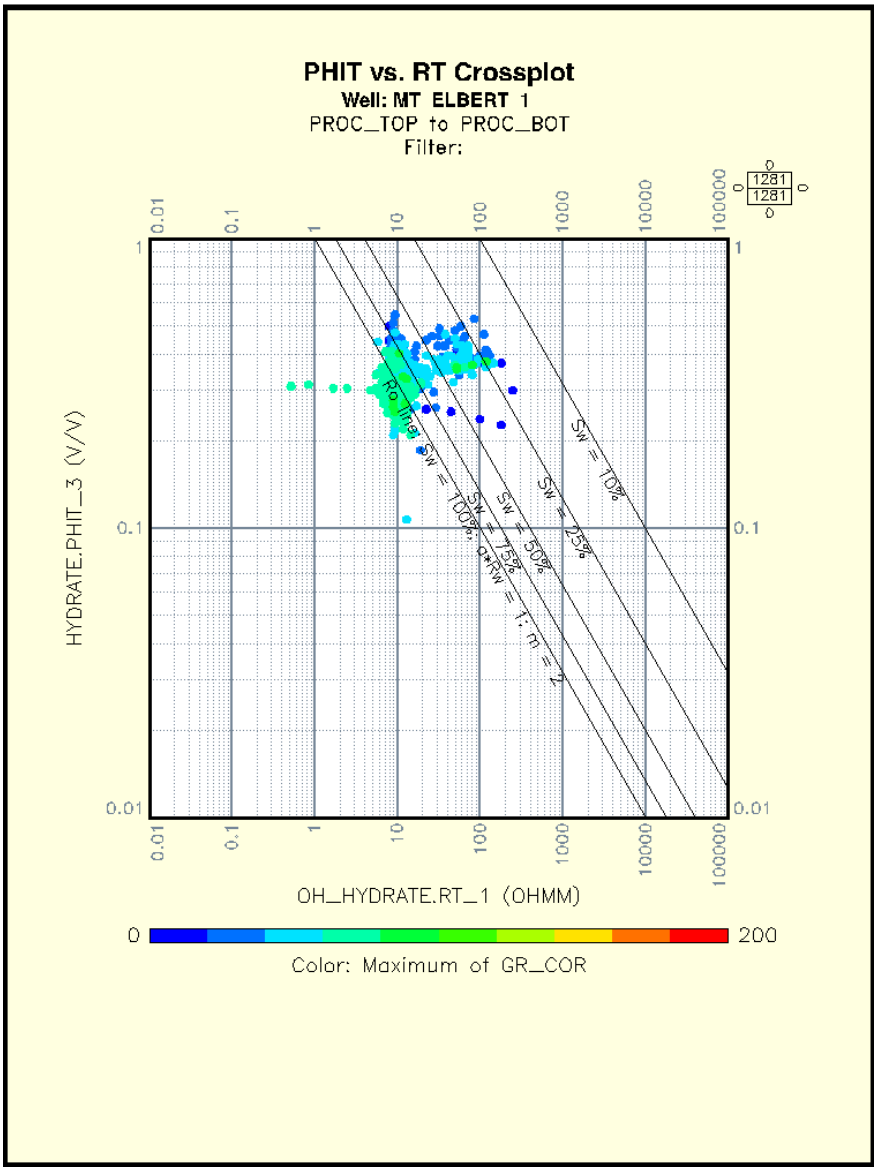

Figure C3. Pickett plot from Mt. Elbert well using a=1, m=2, and n=2 for Archie constants.

Several caveats apply to this method. First, Archie's equation cannot differentiate between free gas, ice, and gas hydrate. Thus, the hydrate saturation values must be studied in conjunction with the downhole logs to match the correct log responses with the correct type of hydrocarbon or water. This is not a significant problem because the downhole log responses of gas hydrate are different from other hydrocarbons. Second, there are several empirical parameters (a, m, and n) and a well specific parameter (R_w) that must be determined. If a water-saturated sandstone (i.e. S_w =1) can be identified, then a reasonable value for R_w can be determined, ignoring the problems of salinity changes during hydrate formation, which are not well understood. In empirical tests, varying R_w by ± 50% resulted in a negligible difference in hydrate saturation estimates. R_w is an important value, but there is some room for error in the estimate of R_w. Even though there are several parameters that need to be determined in order to utilize Archie's equation, they can be reasonably estimated from the downhole well logs. When compared to

other methods, (Williams et al, 2008; Collett, 1998; Collett and Ladd, 2000) Archie's equation proves to be a viable method for making reasonable estimates of hydrate saturation.

4. $$S_w = \left(\frac{a \cdot R_w}{\varphi^m \cdot R_t} \right)^{\frac{1}{n}}$$ Archie's equation (1942)

5. $$S_h = 1 - S_w$$

R_t = Formation resistivity (from log), ohm-m
a = Empirically derived parameter
R_w = Resistivity of formation water, ohm-m
φ = Porosity, volume fraction
m = Empirically derived parameter
S_w = Water saturation, volume fraction
n = Empirically derived parameter
S_h = Saturation hydrate, volume fraction

Simultaneous Equation Solvers

Williams et al., (2008) use Interactive Petrophysics™ (IP) Mineral Solver to determine hydrate saturation. Their approach is unique because hydrate can be entered into the model either as a pore-filling hydrocarbon or as a matrix mineral. Mineral Solver uses a matrix algebra technique called Singular Value Decomposition (SVD) to solve over-determined systems of simultaneous equations. The model requires end-member data for each component of the system (see Table 1), the selected logs from a given well, and a confidence factor for each log which serves to weight the quality of each log. The solver then solves a set of normalized linear equations using the following steps:

1. Each equation is normalized by dividing all terms in the equation by its confidence weighting.
2. The equations are arranged in arrays and solved by matrix algebra using Singular Value Decomposition.
3. If any of the volume result terms are negative then the largest negative term is set to zero and removed from the model. The equation solver is rerun and results again checked for negative terms. This continues until all volumes are positive.
4. The result volumes are adjusted so that they add up to 1.0. Due to the way the equation solver works, the unity equations will not necessarily force the results to absolutely 1.0 therefore the tolerance of the unity equation is set at 0.01 by default.

This method was compared to Archie's equation in the Mallik 5L-38 research well as a test. Williams et al., (2008) found a better correlation with Archie's equation when they used hydrate as a pore-filling parameter (method 1) rather than a matrix component (method 2). However, Williams et al., (2008) note that the correlation with Archie's is better using method 1 because method 1 uses a modified version of Archie's equation to determine hydrate saturation whereas method 2 determines the volume of hydrate and converts it to a saturation by dividing by neutron

porosity. The accuracy of the probabilistic model can only be determined by assuming that other methods produce reliable estimates of hydrate saturation.

	Quartz	Clay	Water	Hydrate
Sonic (μs/m)	250	3286	683	100
Neutron (p.u.)	Auto	0.37	Auto	0.5
Density (gm/cm^3)	2.65	2.7	1.0	0.9
Gamma (API)	50	120	20	20

Table 1. Parameter values used by Williams et al., (2008) in their IP model. No justification for sonic values is given in their paper.

A similar approach utilizes the ConocoPhillips Advanced Interpretation Module (AIM) in Geolog. AIM does not use Archie's equation, but rather is a simultaneous equation solver. Using a table like Williams et al. (2008), end-member values have been defined for water, hydrate, shale, and quartz, using hydrate as a part of the rock matrix. The program integrates input parameters with sonic, gamma ray, density, and neutron porosity measurements to calculate the volume of hydrate present at each sampled log increment. Simple conversion of hydrate volume into hydrate saturation follows. These equations are solved using AIM:

$$6.\ \rho_{bulk} = \rho_{hydrate} \cdot V_{hydrate} + \rho_{shale} \cdot V_{shale} + \rho_{water} \cdot V_{water} + \rho_{quartz} \cdot V_{quartz}$$

$$7.\ NPHI = NPHI_{hydrate} \cdot V_{hydrate} + NPHI_{shale} \cdot V_{shale} + NPHI_{water} \cdot V_{water} + NPHI_{quartz} \cdot V_{quartz}$$

$$8.\ GR = GR_{hydrate} \cdot V_{hydrate} + GR_{shale} \cdot V_{shale} + GR_{water} \cdot V_{water} + GR_{quartz} \cdot V_{quartz}$$

$$9.\ DT = DT_{hydrate} \cdot V_{hydrate} + DT_{shale} \cdot V_{shale} + DT_{water} \cdot V_{water} + DT_{quartz} \cdot V_{quartz}$$

$$10.\ V_{hydrate} + V_{shale} + V_{water} + V_{quartz} = 1$$

	Quartz	Clay	Water	Hydrate
Sonic (μs/ft)	65	140	189	85
Neutron (v/v)	0	0.4	1	0.8
Density (g/cm^3)	2.65	2.6	1	0.91
Gamma (API)	50	120	0	20

Table 2. End-member values used for AIM solver.

Testing the AIM solver on Mt Elbert (Figure C4) and other known hydrate wells proved it can accurately identify known hydrate-bearing intervals and saturations. The biggest limitation of this method is that it needs the four logs listed in Table 2 as inputs and cannot work without all four. The biggest advantage of this method is that no well- or formation-specific parameters, such as R_w, need to be estimated, which makes the module simple to run in batch mode.

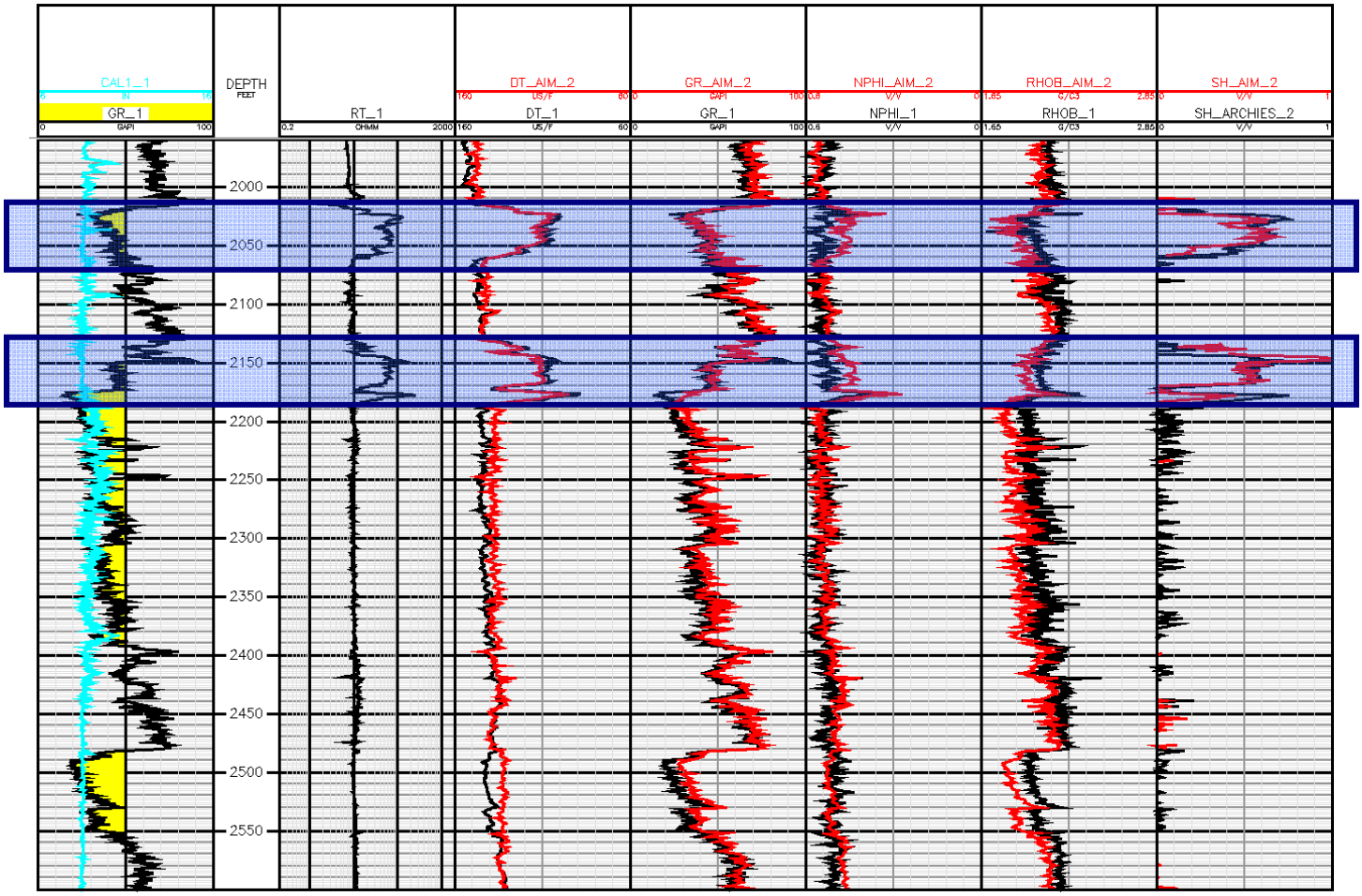

Figure C4. Results for Mt. Elbert well using AIM solver (wireline logs in black, AIM computed logs in red; SH_AIM = hydrate saturation calculated by AIM; SH_ARCHIES = hydrate saturation calculated by Archie's equation using the Humble values for *a*, *m*, and *n* and R_w = 1.2) with hydrate bearing intervals highlighted in blue.

Sonic Methods:

Gomez et al (2008), combine two theoretical models, one that relates to the elastic-wave velocity to porosity, mineralogy, and pore fluid, and another that relates resistivity to porosity and saturation. The two models allow production of "rock-physics templates of the normalized resistivity versus P-wave impedance that serve to solve for porosity and saturation from those two inputs." In other words, Gomez et al (2008) plotted data on a Cartesian plot with P-wave impedance on the x-axis and resistivity on the y-axis, with a secondary mesh that plots porosity versus hydrate saturation (Figure C5). One advantage of this model is that gas rich and water saturated sections plot in distinctively different areas from gas hydrate. This model is henceforth referred to as the Stanford model, since it was developed at Stanford University.

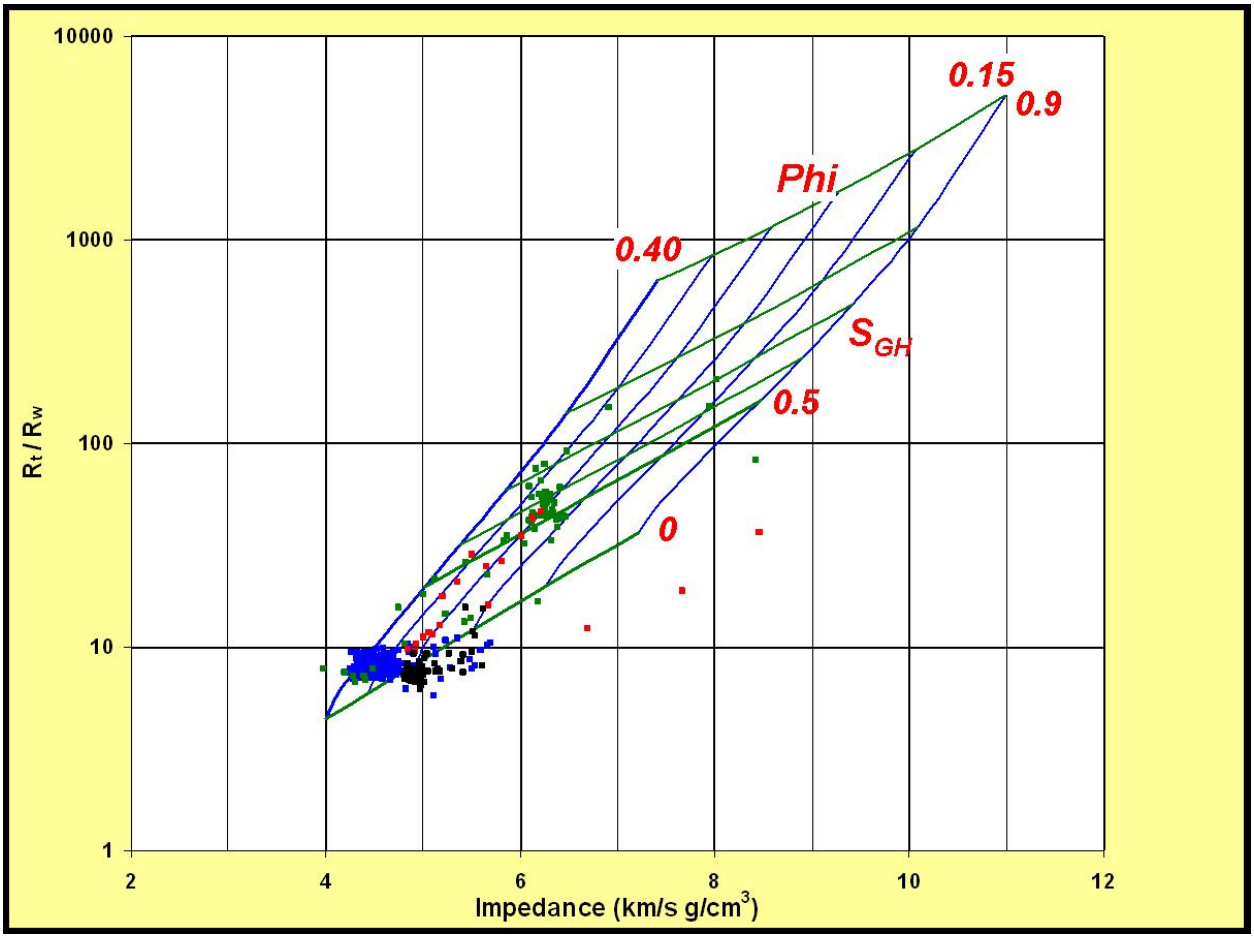

Figure C5. A plot from the Mt. Elbert well "C" sand using the method from Gomez et al (2008).

This model has been shown to be an accurate identifier of gas hydrate saturations, but like the other models, it carries some caveats. The model requires only sonic, density, and deep resistivity logs to calculate hydrate saturation, but if any of these logs is missing, the model is incapable of producing any results. Just as with Archie's equation, the Stanford model requires identification of a water-saturated sand for calculation of apparent resistivity of water (R_{wa}) to accurately compute hydrate saturation. Log data problems can seriously impact the effectiveness of this method and is particularly sensitive to resistivity log problems. Impedance values can be

greatly affected by gas associated with hydrate dissociation. Finally, clay content is not accounted for in preparing the secondary mesh, which may incorrectly estimate hydrate saturation or cause entire intervals to plot off of the secondary mesh, resulting in errors. This model was not implemented in this study.

Another method that utilized P-wave and S-wave velocities was implemented by Lee and Collett (1999). Gas hydrate bearing sediments exhibit elevated acoustic wave velocities compared to pore-filling fluids for both compressional and shear waves. Because of this difference in acoustic velocities, many studies have attempted to estimate gas hydrate saturations using seismic velocities. Lee and Collett (1999) use a series of three-phase equations (the three-phase weighted equation from Lee et al, 1996; the three-phase Wood equation from Wood, 1941; and a three-phase time average equation from Pearson et al, 1983) to determine hydrate saturation using P-wave and S-wave velocities. They tested their approach on the Mallik 2L-38 research well with very good agreement between the P-wave and S-wave approaches for hydrate saturation estimation (39% on average using P-wave data and 37.8% on average using S-wave data).

This method uses several well-specific parameters, including matrix velocities for P-waves and S-waves, a weighting term (W) that is dependent on the clay content of the formation. (Lee and Collett (1999) assume the clay content to be an average of 10%) and the P-wave and S-wave velocities of gas hydrate. These parameters may vary significantly from well to well and may not be easily determined. Lee and Collett (1999) demonstrate that average hydrate saturations vary only 2% with a 30% variation in clay content, and thus conclude that clay content parameter is insignificant so long as it is within a reasonable range of values.

Another sonic method is inversion of the Xu and White method (1995) for determining compressional and shear wave velocities to estimate sonic porosity as outlined in Keys and White (2002). The original Xu and White (1995) paper is a simplification of a method for determining compressional and shear wave velocities by Kuster and Toksoz (1974). The Xu-White model performs the following conceptual steps:

1. Creates a grain comprised of quartz (sand) and shale
2. Adds porosity to the grain
3. Fills the porosity with fluid (water, gas, or oil)

In the Xu-White method, gas hydrate is considered to be part of the rock matrix rather than a pore-filling fluid. Consequently, the Xu-White equation is essentially "blind" to gas hydrate because the rock matrix is composed of only sand and shale. In the absence of gas hydrate, porosities predicted by the Xu-White method match CMR-derived does very well (Figure C6). As in Kleinberg and Flaum's (2005) NMR method, separation between of density porosity and sonic porosity is an indicator of hydrate occurrence. An attempt was made, using Equation 2, to calculate hydrate saturation by replacing total CMR porosity (TCMR) with calculated sonic porosity (Figure C7). Results appear to underestimate hydrate saturation by as much as 20%. This underestimation is a direct result of Xu-White being a two end-member model (sand and shale). The sonic porosity is not equal to the NMR porosity and thus Equation 11 does not make a correct estimate of hydrate saturation from sonic porosity. Since the sonic tool "sees" hydrates

as part of the matrix and not a pore-filling fluid, the Xu-White model is unable to account for all of the hydrate present. The sonic porosity method is an accurate identifier of hydrate intervals and is a powerful tool for eliminating noise from other methods because the sonic porosity model makes more conservative hydrate saturation estimates and is less prone to identifying false hydrate.

$$11.\ S_h = \frac{DPHI - PHIMOD}{DPHI + \alpha \cdot PHIMOD}$$

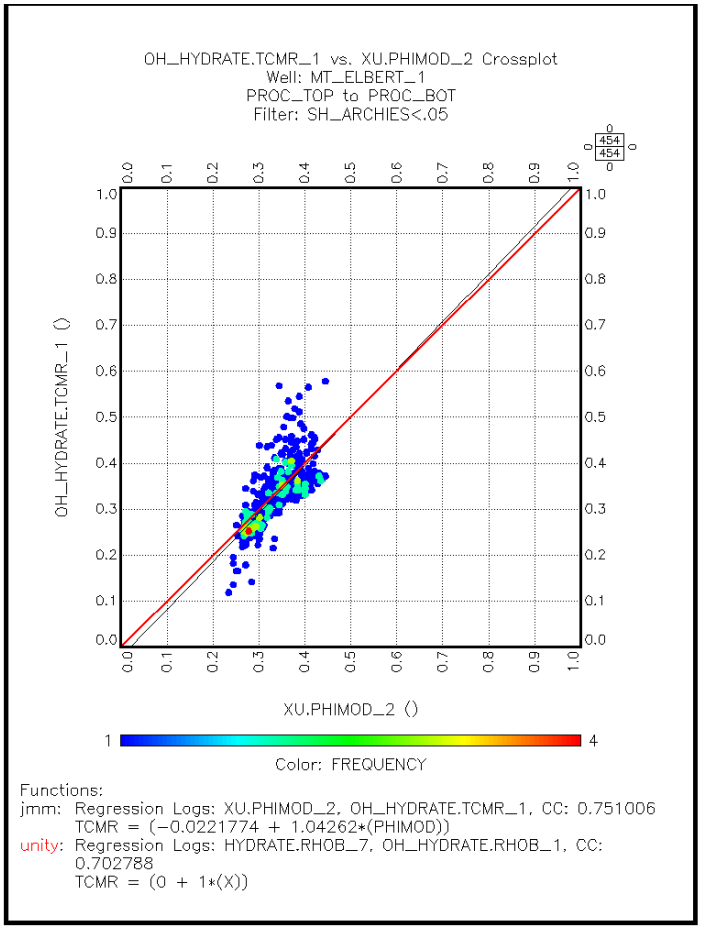

Figure C6. CMR porosity versus Xu-White sonic porosity cross plot from Mt. Elbert well (1:1 line in red, regression in black) with hydrate intervals excluded. The plot shows excellent agreement between the two and can be seen in Figure C7 below as well.

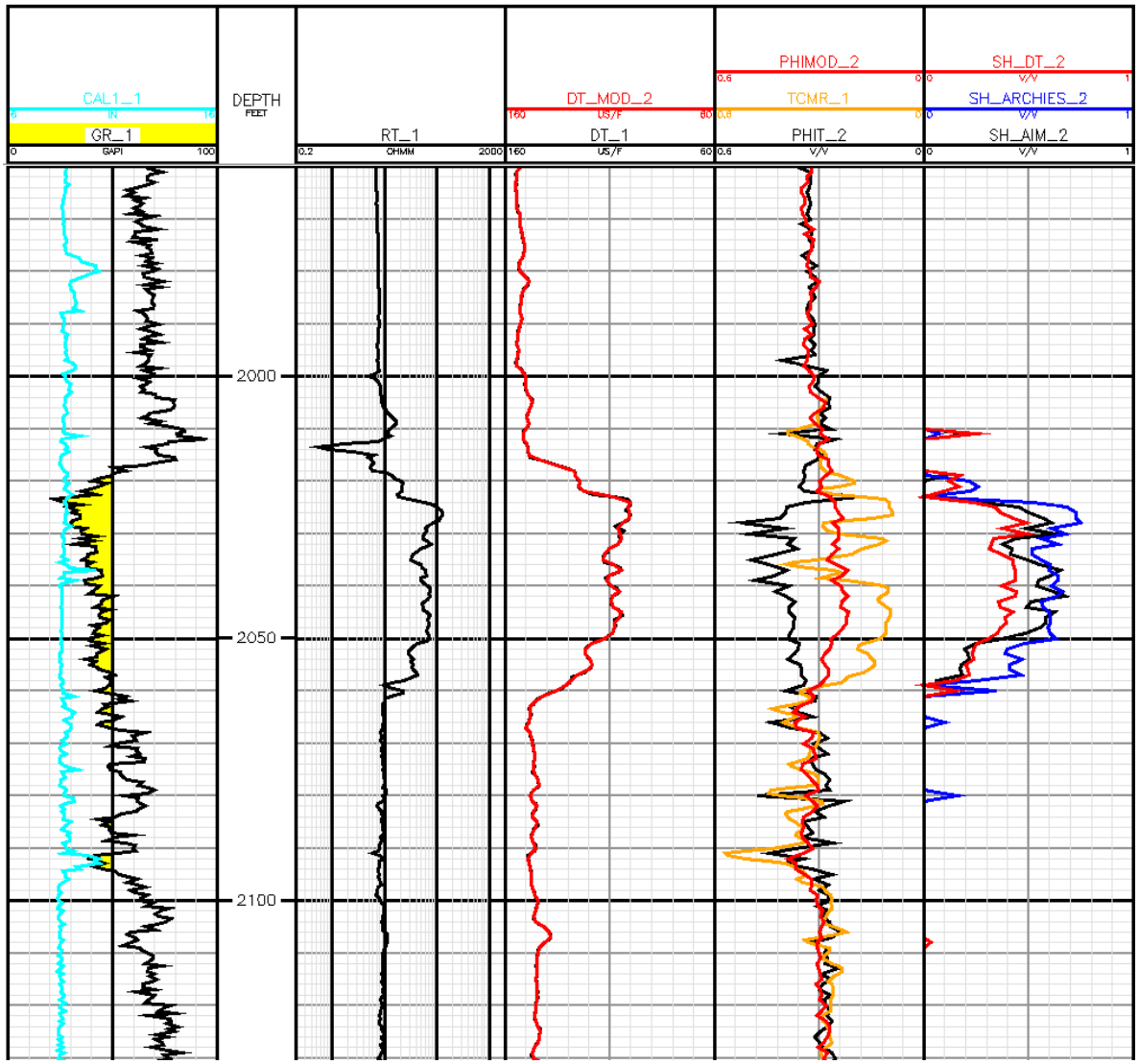

Figure C7. Inverse Xu-White model results displayed for Mt. Elbert well (DT_MOD = Modeled sonic log; PHIMOD = modeled sonic porosity; SH_DT = hydrate saturation calculated by sonic porosity method).

Hydrate Saturation Module:

A hydrate saturation module was created within Geolog to determine hydrate location and saturation. Based upon the methods described above for determining hydrate saturation, one method from each category was selected and implemented in the hydrate saturation module. The module uses wireline logs to compute hydrate saturation with as many of the four methods as possible. If a log is missing that is needed to compute a given method, then that method will calculate and output a hydrate saturation equal to zero. The methods chosen to calculate hydrate saturation are: Kleinberg et al. (2005) NMR method, Archie's equation, the AIM simultaneous solver, and the Xu-White sonic method. If AIM module is going to be utilized, AIM must be run before the hydrate module. If the Xu-White model is used, it must be run *after* the hydrate

module because it requires clay volume as an input (which is computed by the hydrate module). After the hydrate module is run, the Xu-White model can be run, followed by the hydrate module again, which will yield a sonic porosity hydrate saturation.

The hydrate saturation module first computes clay and sand "end-members" for each well from the gamma ray. These points are then used to calculate the clay volume for each well. The module then calculates density porosity with an optional clay correction. In this study of North Slope wells, density porosity and CMR porosity have nearly a 1:1 agreement (Figure C8), so a clay correction was not applied. In wells where the density curve was missing, a synthetic density curve was created. The calculated density curve is based on a cross-plot of density and clay volume and is shown to emulate the density curve quite well (Figure C9). Hydrate saturation is then calculated by Archie's equation, the AIM simultaneous solver, and the Xu-White sonic method. Finally, several flags are generated, including a coal flag (with user controlled cut-off parameters), a possible hydrate flag (for when one or more hydrate indicating logs are missing) and a definite hydrate flag (for when multiple methods indicate gas hydrate).

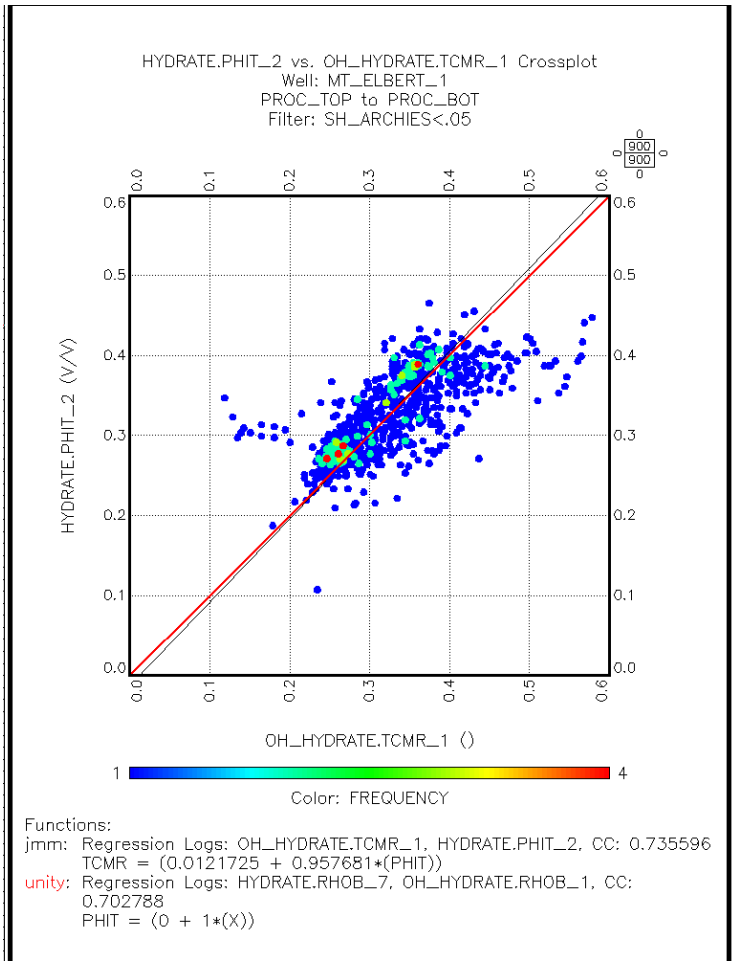

Figure C8. Plot of computed density porosity (PHIT) versus CMR porosity for the Mt. Elbert well (data points colored by frequency. 1:1 line in red and regression line in black) The near 1:1 correlation justifies the use of the density porosity calculation without a clay correction.

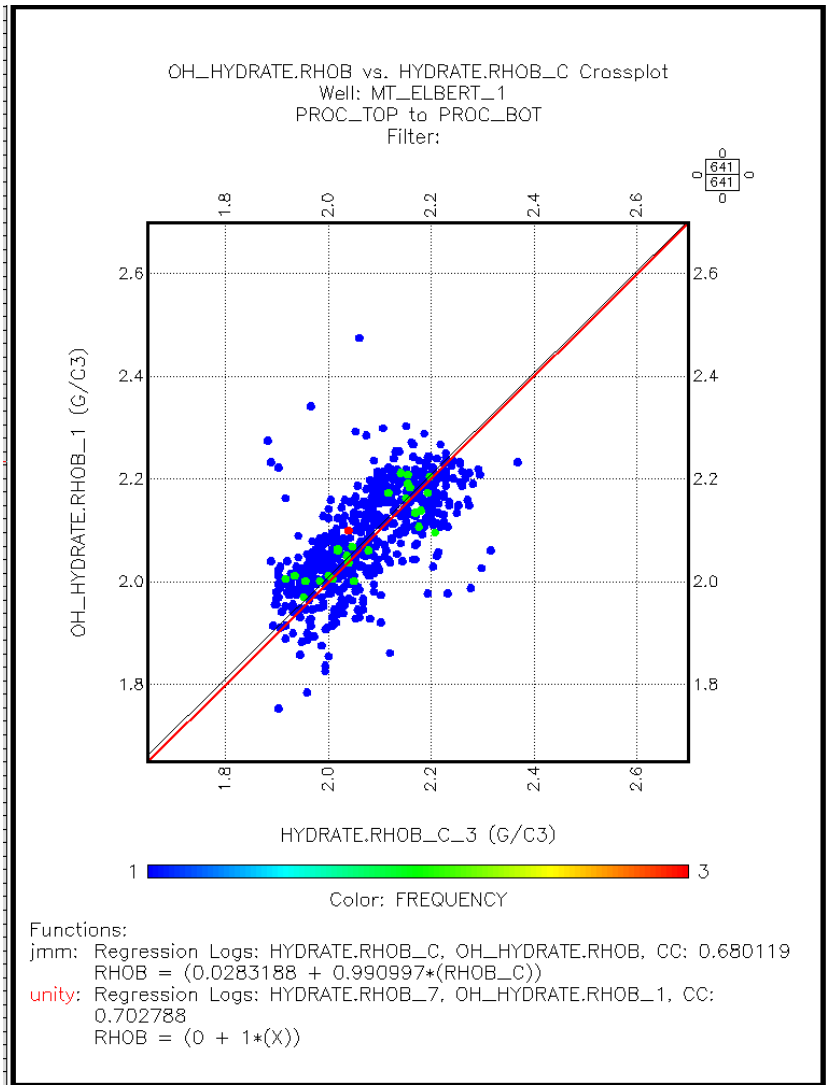

Figure C9. RHOB versus calculated RHOB curve based on clay volume (1:1 line in red, regression line in black, data points colored by frequency) shows near 1:1 correlation.

Results:

Seventeen wells on the North Slope of Alaska were analyzed for hydrate occurrence using the Hydrate Saturation Module developed in Geolog in this study. The fundamental challenge with these wells was that none of them were drilled with the explicit purpose of looking for gas hydrates and thus many of the wells did not have a complete log suite through the Gas-Hydrate Stability Zone (GHSZ.) Of the 17 wells analyzed, W KUP 3-11-11 and L-106 have the best evidence of hydrate occurrence. Both wells have wireline log responses similar to Mt. Elbert, NW Eileen St. 2, and Mallik 5L-38 which are all known to contain gas hydrate-bearing strata. The hydrate saturation module also indicates a high level of hydrate saturation (50-70%) in two intervals in W KUP 3-11-11 and four intervals in L-106. Hydrate is indicated in both wells by three methods (AIM, sonic, and Archie's), with no NMR log to confirm the fourth method. Other wells have large quantities of potential hydrate, but are missing one or more logs to verify Archie's method. See Table 3 for a complete summary of the wells analyzed by the hydrate saturation module and Appendix C1 for log plots of a selection of these wells.

Conclusions & Recommendations:

To accurately determine gas hydrate location and saturation on the North Slope of Alaska, a suite of common downhole logs including caliper, gamma ray, sonic, resistivity, density and neutron porosity logs is required. Using these six logs, hydrate saturation can be determined using Archie's equation and the AIM simultaneous equation solver. The Xu-White sonic method can accurately identify hydrate-bearing intervals, but tends to underestimate hydrate saturation. Sonic methods must be accompanied by at least one of the other methods to calculate accurate saturation values. Sonic methods have utility in identifying hydrate-bearing intervals, which is quite useful since it serves as a check to see if the other methods are registering false hydrate saturation. The magnetic resonance method for hydrate determination is likely the most accurate method, but NMR logs are not often run in the gas hydrate stability zone, limiting the utility of this method. In future wells are drilled specifically for hydrate testing and/or exploitation, sonic log and/or NMR log is strongly recommended. Magnetic resonance techniques do not require well-specific parameters and provide the most straightforward method to calculate hydrate saturation, but sonic logs have arguably greater overall utility for other work (e.g. the study of seismic data).

North Slope Well Summaries

Importance Level	Well name	Interval of interest	Additional Comments
Hydrate indicated by 3 different methods			
1	W KUP 3-11-11	2050-2100	Archie's, AIM, Xu-White show hydrate; interesting break in DT at 2070; typical RT and DT hydrate response.
		2245-2280	Archie's, AIM, Xu-White show hydrate; typical RT and DT hydrate response; possibly best interval for hydrate
1	L-106	1920-1950	Archie's, AIM, Xu-White show hydrate; typical RT and DT hydrate response.
		2060-2120	Archie's, AIM, Xu-White show hydrate; typical RT and DT hydrate response.
		2255-2290	Archie's, AIM, Xu-White show hydrate; typical RT and DT hydrate response.
		2330-2370	Archie's, AIM, Xu-White show hydrate; typical RT and DT hydrate response.
Possible hydrate, sonic log would be helpful -- merits further investigation			
2	1H-06	1770-1820	small Rt response; no sonic log present; could just be permafrost
		1980-2000	RT response , no DT log. DPHI≈NPHI. Archie's shows hydrate saturation of 50+%. Deeper response is Ungu
2	NWE 1-01	2430-2475	Archie's shows hydrate. Strong Rt response, similar to W KUP 3-11-11
2	W SAK 24	2260-2280	Archie's shows hydrate, could be casing response. Neutron-density cross-over below interval
2	NWE 2-01	1950-2100	Archie's shows hydrate; strong Rt response; limited sonic log
Possible, but unlikely hydrate			
3	KUP ST 7-11-12	1860-1940	RT and DT response; could still be permafrost; RT-DT x-plot does not indicate hydrate
		2850-2900	Rt response but no sonic response. RT-DT x-plot does not indicate hydrate
3	CHEV 18-11-12	2855-2915	Rt response, sonic log is present, but unusuable. Neutron-density cross-over in interval of interest
3	3M-09	2075-2125	RT and DT response - low hydrate saturation? Deeper responses coincide with Ugnu interval
Shows explainable false hydrate			
4	1J-09	2175-2250	Large RT response, slow sonic response -- neutron density cross-over, unlikely to be hydrate
4	1Q-101	1875-1945	Neutron density cross-over at various intervals; no appropriate RT, DT response for hydrate
4	1D-05	2280-2370	Neutron density cross-over; no sonic response
5	1C-01	2050-2100	Archie's shows some hydrate, no DT response
No response			
5	3C-06	None	Archie's shows insignificant amounts of hydrate due to small RT response
5	2D-15	None	Archie's shows no hydrate, no RT and/or DT response
5	1C-05	None	Archie's shows no hydrate, no RT and/or DT response
5	1F-05	None	Archie's shows no hydrate, no RT and/or DT response

Table 3. A complete summary of the well log analysis of the 17 wells that were analyzed using the Hydrate Saturation Module

References:

Anderson, B.I. and Collett, T.S., 2008, Open Hole and Cased-Hole Resistivity Logs to Monitor Gas Hydrate Dissociation During a Thermal Test in the Mallik 5L-38 Research Well, Mackenzie Delta, Canada, Petrophysics, v. 49, no/ 3, pp. 285-294.

Archie, G.E., 1942, The electrical resistivity log as an aid in determining some reservoir characteristics, Journal of Petroleum Technology, v. 5, pp. 1-8.

Boswell, R., Hunter, R., Collett, T., Digert, S., Hancock, S. and Weeks, M., 2008, Investigation of Gas Hydrate-Bearing Sandstone Reservoirs at the "Mount Elbert" Stratigraphic Test Well, Milne Point, Alaska. Proceedings of the 6th International Conference on Gas Hydrates (ICGH 2008), Vancouver, British Columbia, CANADA, July 6-10, 2008.
http://www.netl.doe.gov/technologies/oil-gas/publications/2008_ICGH/ICGH_5755_41332.pdf

Collett, T.S., 1998, Well log evaluation of gas hydrate saturations, SPWLA 39th Annual Logging Symposium.

Collett, T.S. and Ladd, J., 2000, Detection of gas hydrate with downhole logs and assessment of gas hydrate concentrations (saturations) and gas volumes on the Blake Ridge with electrical resistivity logs. In: Paull, C.K., Matsumoto, R., Wallace, P.J., and Dillion, W.P. (Editors), Proceedings of the Ocean Drilling Program, Scientific Results, v. 164.

Collett, T.S., 2001, A Review of Well-Log Analysis Techniques Used to Assess Gas-Hydrate Bearing Reservoirs, AGU, Geophysical Monograph 124.

Gomez, C.T., Dvorkin, J., and Mavko, G., 2008, Estimating the hydrocarbon volume from elastic and resistivity data: A concept, The Leading Edge, June 2008.

Graue, A., Kvamme, B., Stevens, J., and Howard, J., 2006, Magnetic Resonance Imaging of Methane – Carbon Dioxide Hydrate Reactions in Sandstone Pores, SPE, Annual Technical conference.

Hesse, R., Frape, S.K., Egeberg, P.K., and Matsumoto, Ryo, 2000, Stable isotope studies (Cl, O, and H) of interstitial waters from site 997, Blake Ridge gas hydrate field, West Atlantic, pp. 129-137. In: Paull, C.K., Matsumoto, R., Wallace, P.J., and Dillon, W.P., (editors), Proceedings of the Ocean Drilling Program, Scientific Results, v. 164

Keys, R.G. and Xu, S., 2002, An approximation for the Xu-White velocity model, Geophysics, v. 67, no.5, pp. 1406-1414.

Kleinberg, R.L., Flaum, C., Griffin, D.D., Brewer, P.G., Malby, G.E., Peltzer, E.T., and Yesinowski, J.P., 2003, Deep Sea NMR: Methane hydrate growth habit in porous media and its relationship to hydraulic permeability, deposit accumulation, and submarine slope stability, Journal of Geophysical Research, v.108, no. B10, 2508.

Kleinberg, R.L., Flaum, C., and Collet, T.S., 2005, Magnetic resonance log of Mallik 5L-38: Hydrate saturation, growth habit, and relative permeability. In: S.R. Dallimore and T.S. Collett (Editors), Scientific Results from the Mallik 2002 Gas Hydrate Production Research Well, Mackenzie Delta, Northwest Territories, Canada, Bulletin 585. Geological Survey of Canada, Ottawa.

Kuster, G.T. and Toksoz, M.N., 1974, Velocity and attenuation of seismic waves in two-phase media: Part II. Experimental results, Geophysics, v. 39, no. 5, pp. 607-618.

Kvenvolden, K.A., 1988, Methane hydrate – a major reservoir of carbon in the shallow Geosphere?: Chemical Geology, v. 71, pp. 51-51

Kvenvolden, K.A., 1993, Gas hydrates – Geological perspective and global change: Reviews of Geophysics, v.31, no. 2, May, pp. 173-187.

Lee, M.W., Hutchinson, D.R., Collett, T.S., and Dillon, W.P., 1996, Seismic velocities for hydrate-bearing sediments using weighted equation, Journal of Geophysical Research, v. 101, pp. 20347-20348.

Lee, M.W. and Collett, T.S., 1999. Amount of gas hydrate estimated from compressional and shear-wave velocities at the JAPEX/JNOC/GSC Mallik 2L-38 gas hydrate research well; in Scientific Results from JAPEX/JNOC/GSC Mallik 2L-38 Gas Hydrate research well, Mackenzie Delta, Northwest Territories, Canada, (ed.) S.R. Dallimore, T. Uchida, and T.S. Collett; Geological Survey of Canada, Bulletin 544, pp. 313-322.

Lee, M.W. and Collett, T.S., 2001, Controls on the Physical Properties of Gas-Hydrate-Bearing Sediments Because of the Interaction Between Gas Hydrate and Porous Media. Geophysical Monograph, v. 124, pp. 179-187.

Miyairi, M., Akihisa, K., Uchida, T, Collett, T.S., and Dallimore, S.R., 1999, Well-log Interpretation of gas-hydrate bearing formations in the JAPEX/JNOC/GSC Mallik 2L-38 Gas Hydrate research well: in Scientific Results from JAPEX/JNOC/GSC Mallik 2L-38 Gas Hydrate research well, Mackenzie Delta, Northwest Territories, Canada, (ed.) S.R. Dallimore, T. Uchida, and T.S. Collett; Geological Survey of Canada, Bulletin 544, pp. 281-293.

The Mallik 2002 Consortium: Drilling and Testing a Gas Hydrate Well**,** DE-AC26-01NT41007. Accessed in April, 2009 from: http://www.netl.doe.gov/technologies/oil-gas/FutureSupply/MethaneHydrates/projects/DOEProjects/Mallik-41007.html

Pearson, C.F., Halleck, P.M., McGurle, P.L., Hermes, R., and Matthews, M., 1983, Natural gas hydrate: a review of in situ properties, Journal of Physical Chemistry, v. 87, p. 4180-4185.

Prensky, Steven, 1995, A Review of Gas Hydrates and Formation Evaluation of Hydrate-Bearing Reservoirs, SPWLA 36th Annual Logging Symposium.

Sloan, E.D., 1990, Clathrate hydrates of natural gases, Marcel Dekker, Inc., New York, 641 p.

Stevens, J., Howard, J.J., Baldwin, B.A., Ersland, G., Husebo, J., and Graue, A., 2008, Experimental hydrate formation and gas production scenarios based on CO_2 sequestration, Proceedings of the 6th International Conference on Gas Hydrates.

Williams, F., Lovell, M., Brewer, T., Buecker, C., Jackson, P., Camps, A., 2008, Formation evaluation of gas hydrate bearing sediments, SPWLA 49th Annual Logging Symposium.

Williams, T., Millheim, K., Liddell, B., 2005, Methane Hydrate Production from Alaskan Permafrost, DE-FC26-01NT41331. http://www.netl.doe.gov/technologies/oil-gas/publications/Hydrates/pdf/Project_pdfs/FG013105_final_report.PDF

Wood, A.B., 1941 A text book of sound, Macmillan, New York, New York, 578 p.

Xu, S. and White, R., 1995, Poro-elasticity of clastic rocks: a unified model, SPWLA 36th Annual Logging Symposium, June 26-29.

Appendix C1: Well log plots for selected wells that were analyzed in this study.

A. <u>Known hydrate wells</u>: These wells are known to contain gas hydrates

1. Indicate presence of hydrate by three or more methods (Archie's, NMR, sonic, and AIM)
2. Definite hydrate present = dodger blue hydrate flag
3. RHOB-DT crossover (shaded in dodger blue) indicative of hydrate

Mt. Elbert:

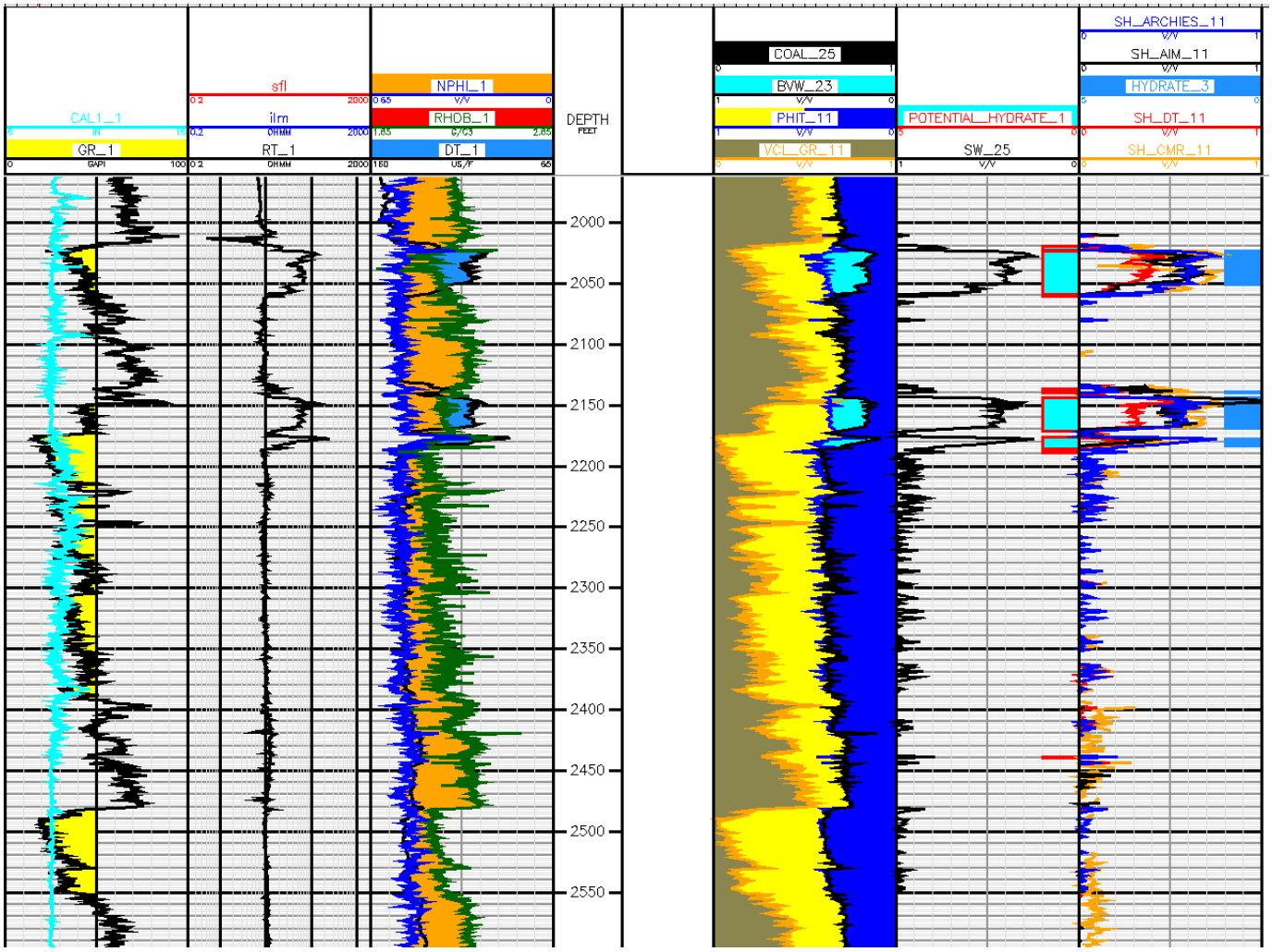

NW Eileen St. 2:

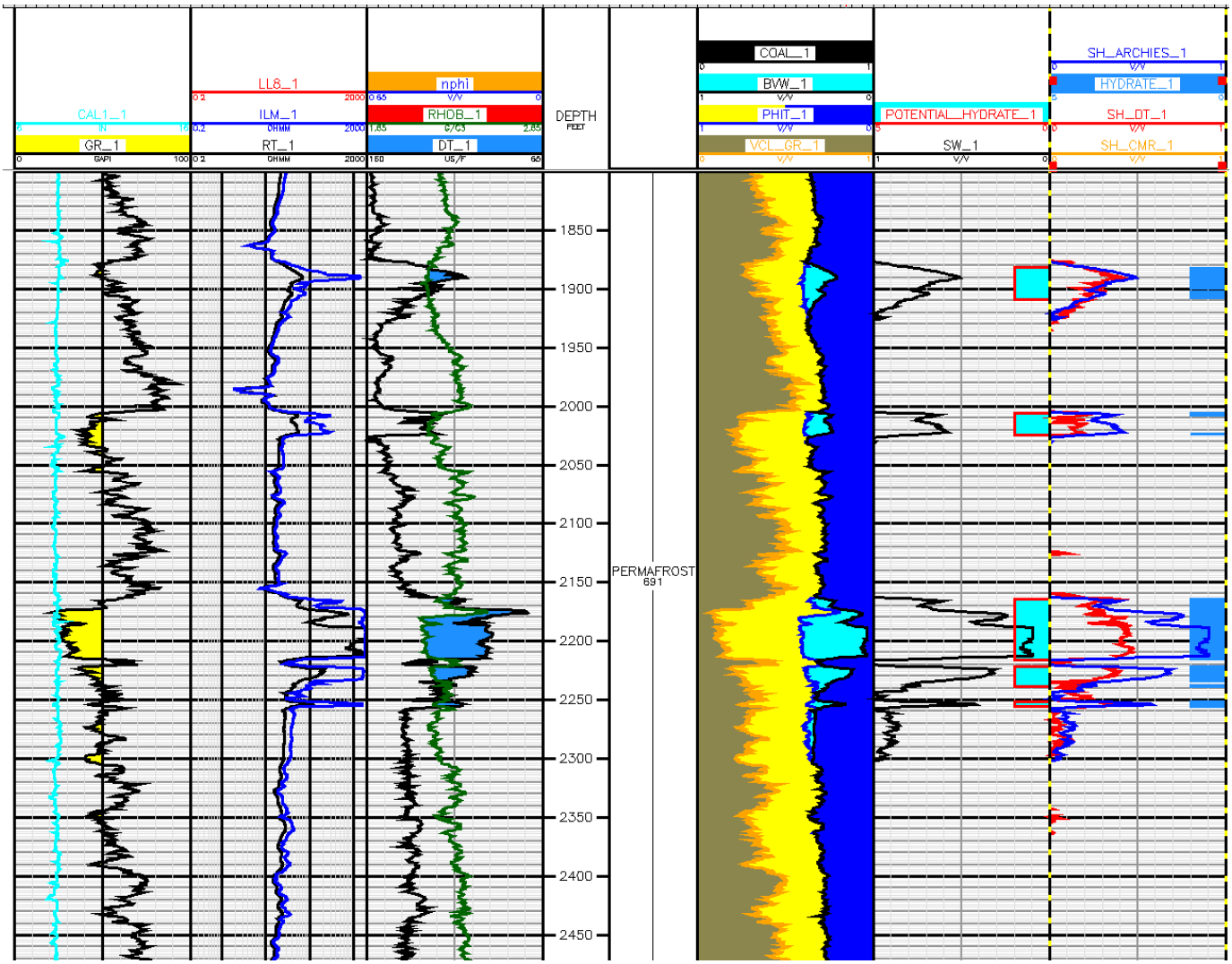

Mallik 5L-38

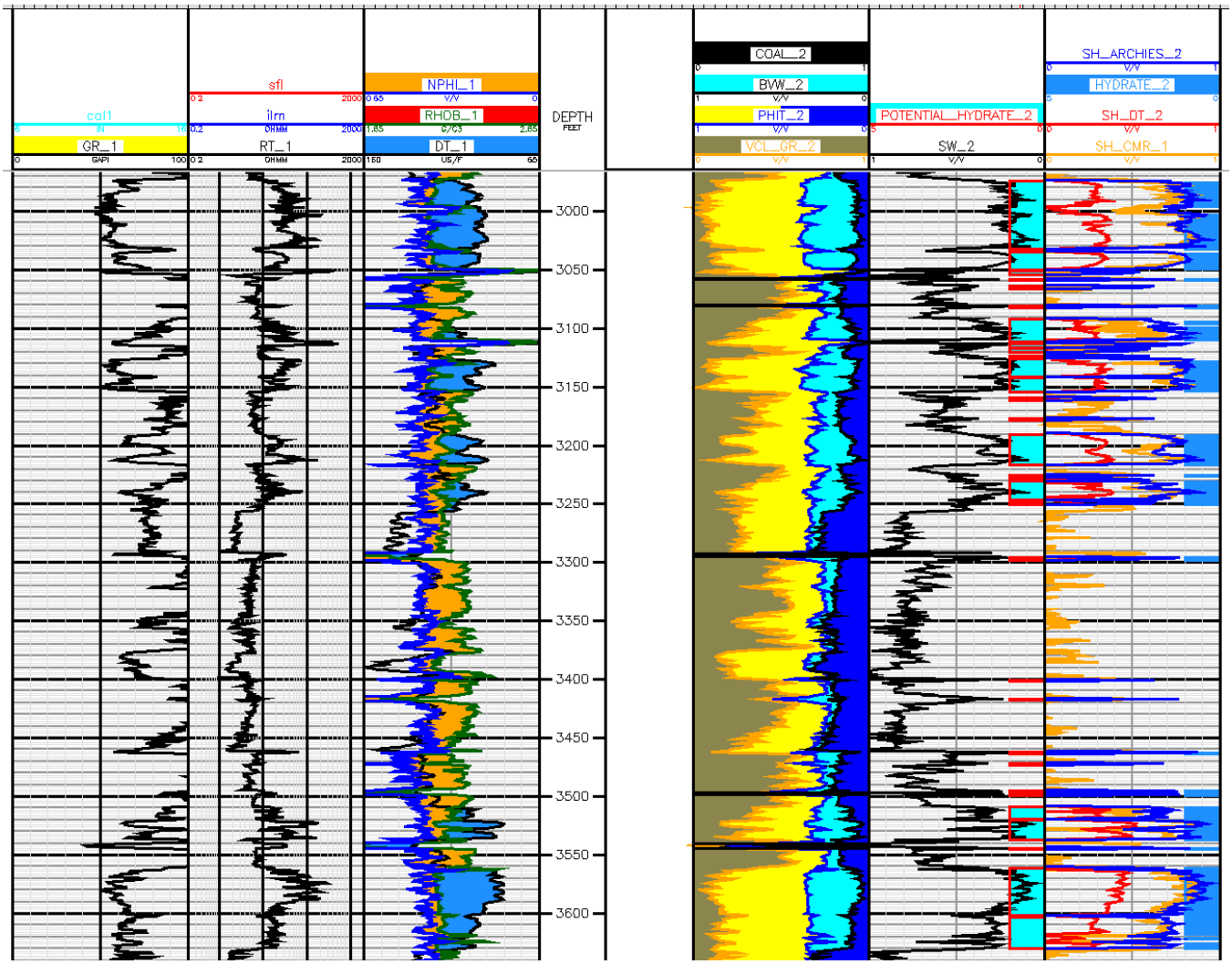
cal1
GR_1
sfl
ilrm
RT_1
NPHI_1
RHDB_1
DT_1
DEPTH
FEET
COAL_2
BVW_2
PHIT_2
VCL_GR_2
POTENTIAL_HYDRATE_2
SW_2
SH_ARCHIES_2
HYDRATE_2
SH_DT_2
SH_CMR_1
3000
3050
3100
3150
3200
3250
3300
3350
3400
3450
3500
3550
3600

B. <u>Inferred hydrate wells</u>: These wells shows the same response as above wells

1. Indicate presence of hydrate by three methods (Archie's, sonic, and AIM)
2. Definite hydrate present = dodger blue hydrate flag
3. RHOB-DT crossover (shaded in dodger blue) indicative of hydrate, in this case the RHOB curve was missing over the interval of interest and the computed RHOB curve was used.

W KUP 3-11-11

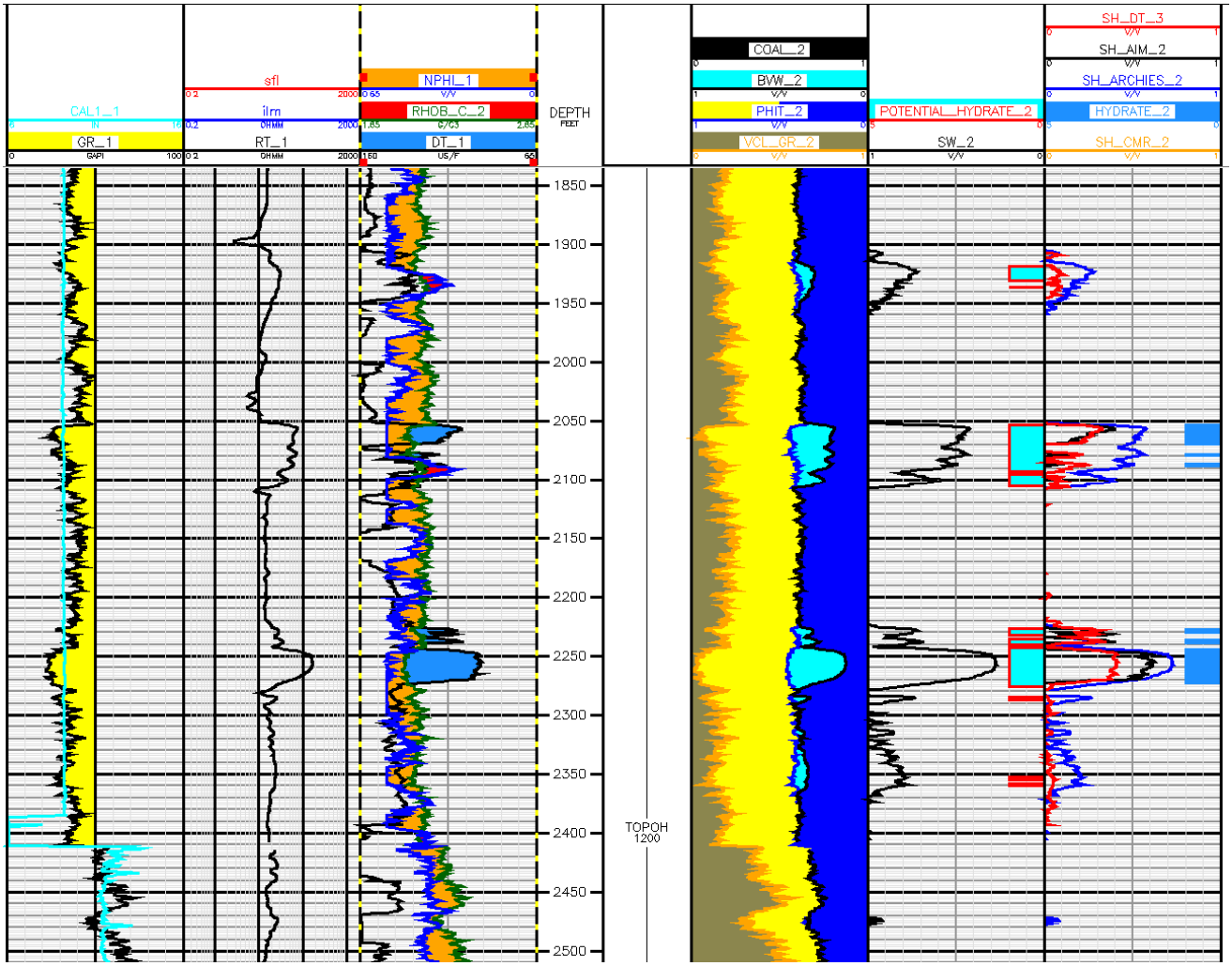

L-106

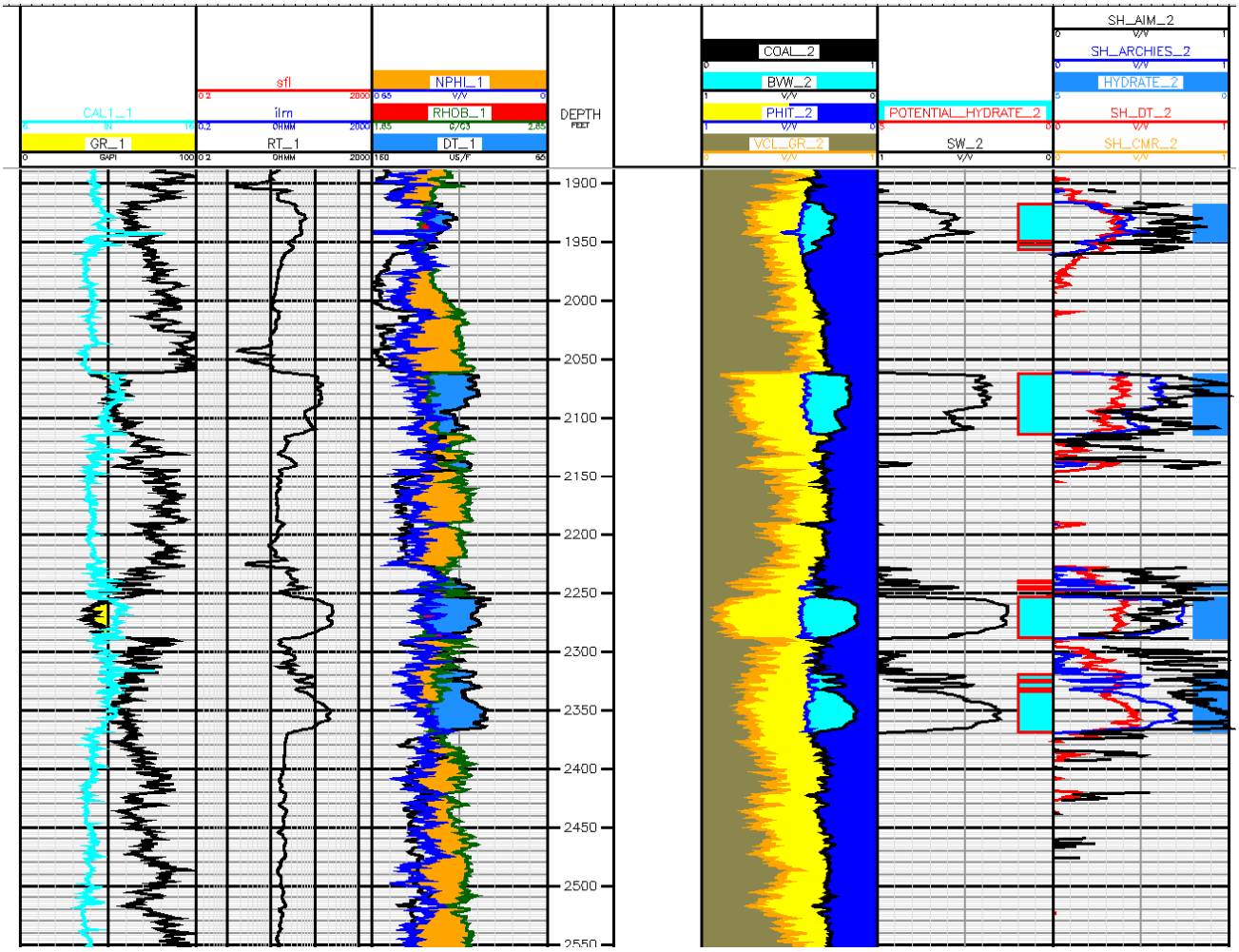
CAL1__1
GR__1
sfl
ilrn
RT__1
NPHI__1
RHOB__1
DT__1
DEPTH
FEET
COAL__2
BVW__2
PHIT__2
VCL_GR__2
POTENTIAL_HYDRATE__2
SW__2
SH_AIM__2
SH_ARCHIES__2
HYDRATE__2
SH_DT__2
SH_CMR__2
1900
1950
2000
2050
2100
2150
2200
2250
2300
2350
2400
2450
2500
2550

C. <u>Possible hydrate wells</u>: these wells may or may not contain hydrate.

1. Hydrate Saturation Module is often inconclusive due to logs missing (most often the sonic log), but hydrate is indicated by at least 1 method.
2. Possible hydrate is indicated in light blue in the lithology track and by a light blue possible hydrate flag.

NWE 1-01

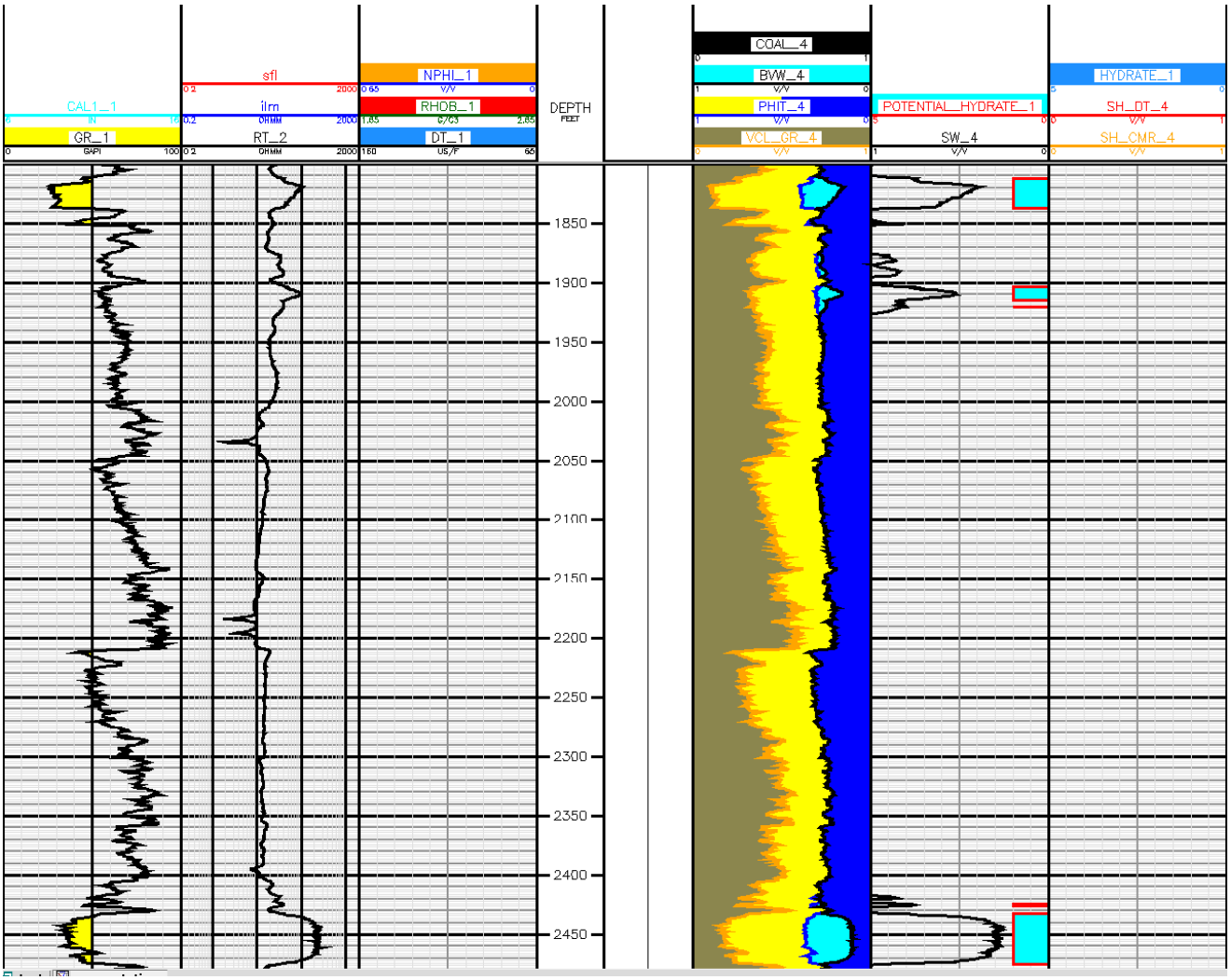

1. This well indicates possible hydrate intervals, but lacks a sonic log over the interval of interest to verify hydrate with classic sonic response and/or other methods. 2425'-2475' is a particularly interesting interval.

D. <u>False hydrate wells</u>: These wells indicate hydrate by Archie's equation, but do not exhibit classic hydrate responses by one or more logs. May have RHOB-NPHI crossover in interval of interest, indicating gas rather than hydrate.

1J-09

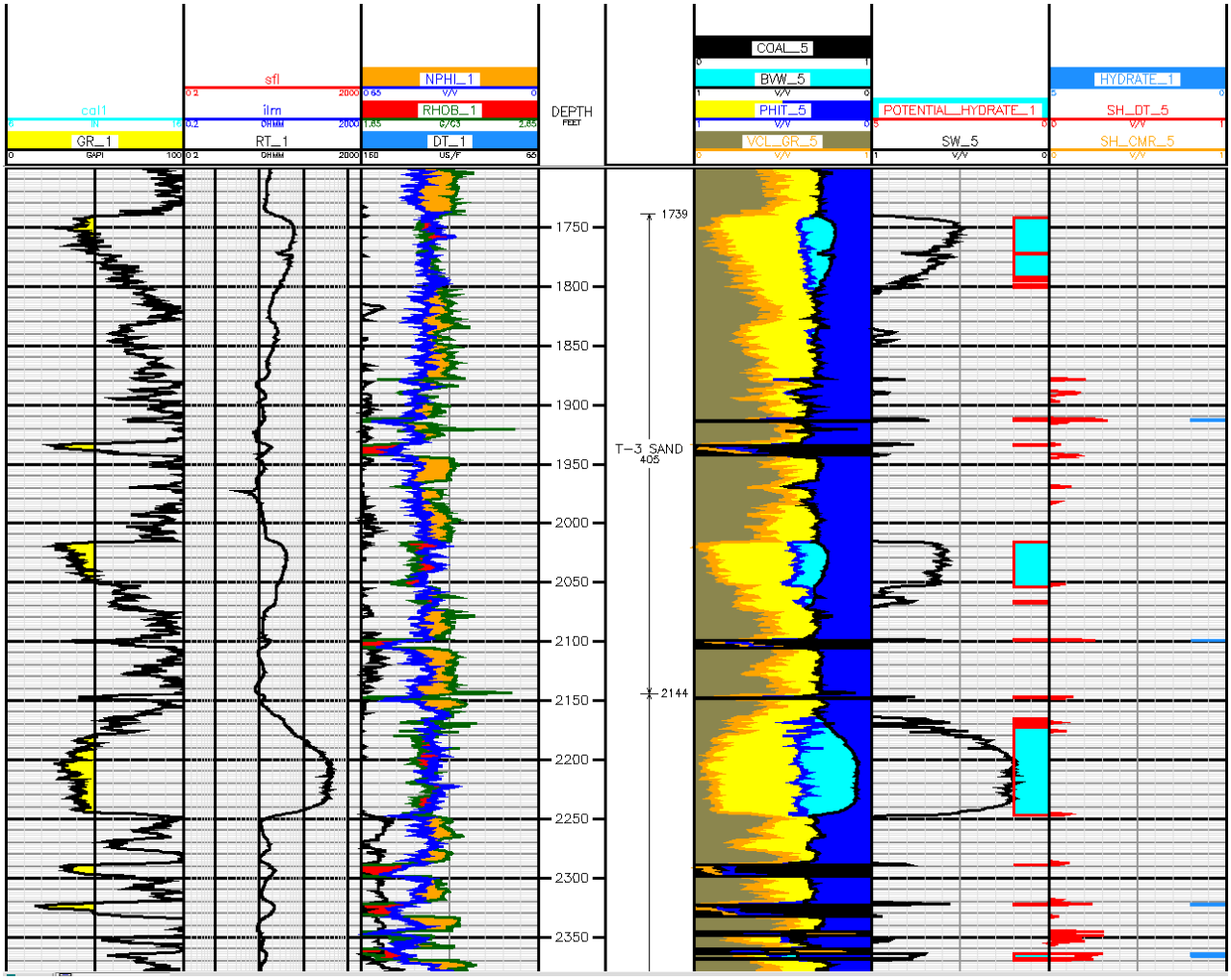

1. Strong resistivity response, but no sonic response
2. No RHOB-DT crossover

1Q-101

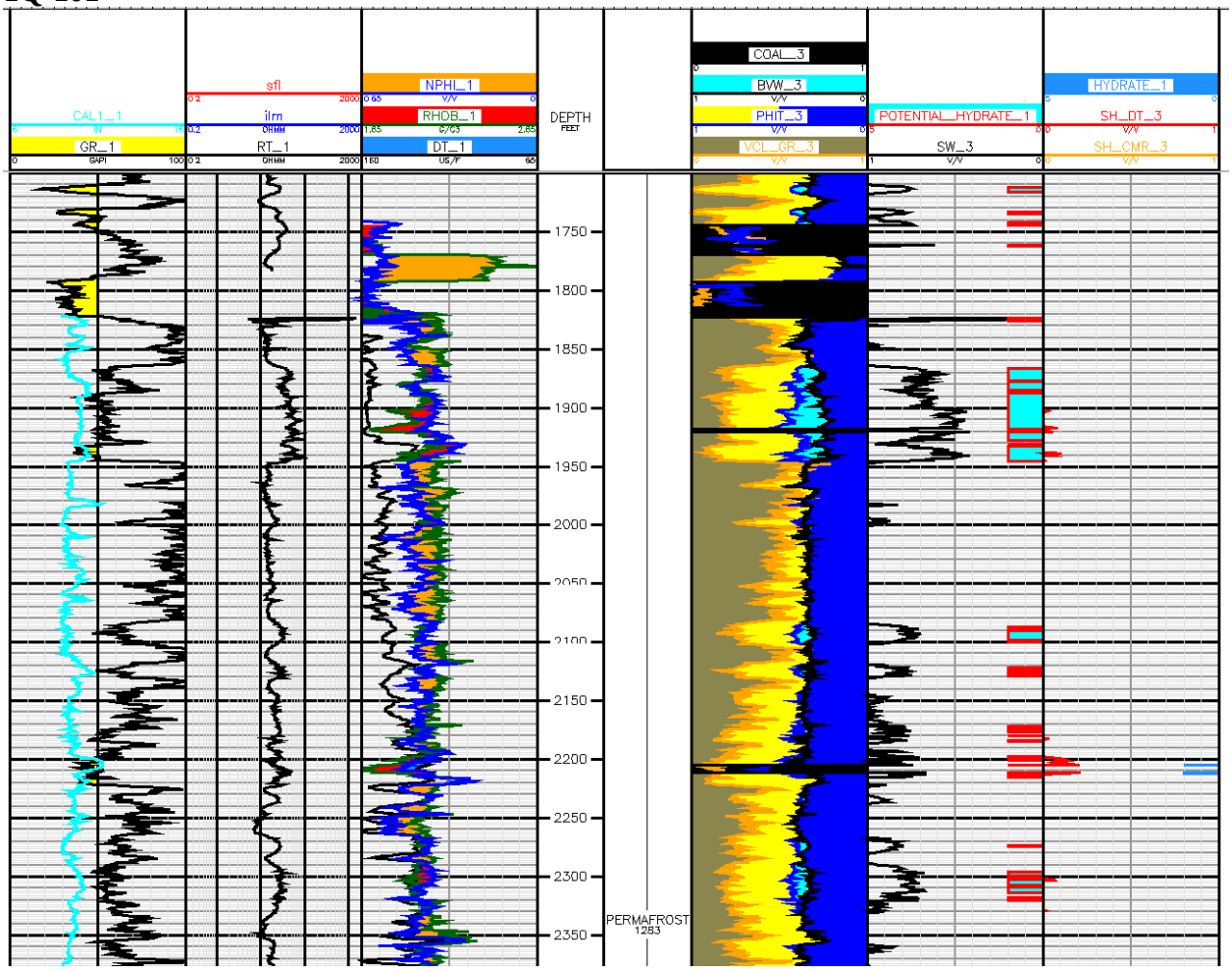

1. RHOB-NPHI (shaded in red) crossover indicative of gas, not hydrate

Chev 18-11-12

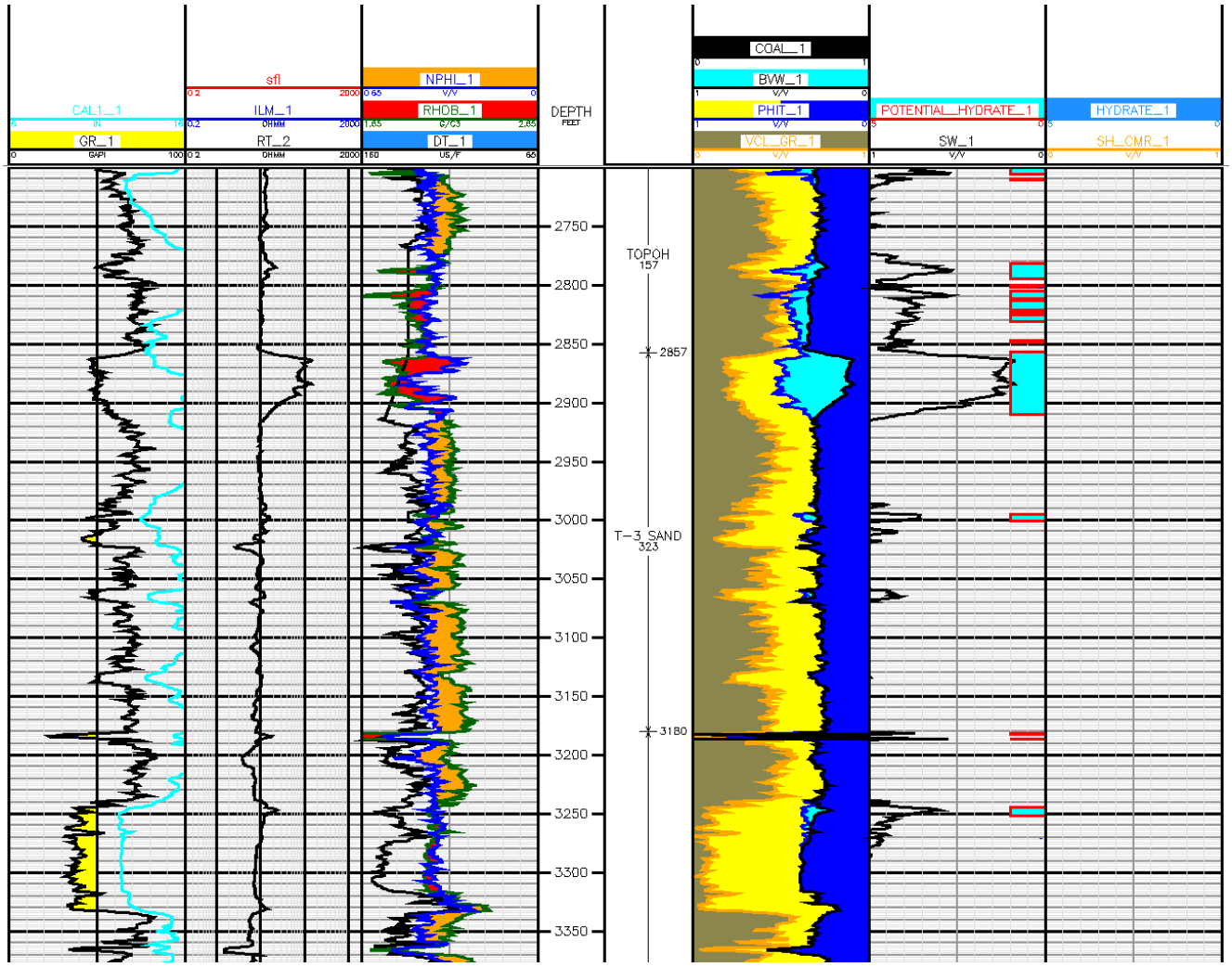

1. Sonic log is unusable in interval of interest
2. RHOB-NPHI crossover (shaded in red) indicative of gas, not hydrate

E. <u>Wells that do not contain hydrate</u>: These wells show no indication of gas hydrate occurrence

2D-15

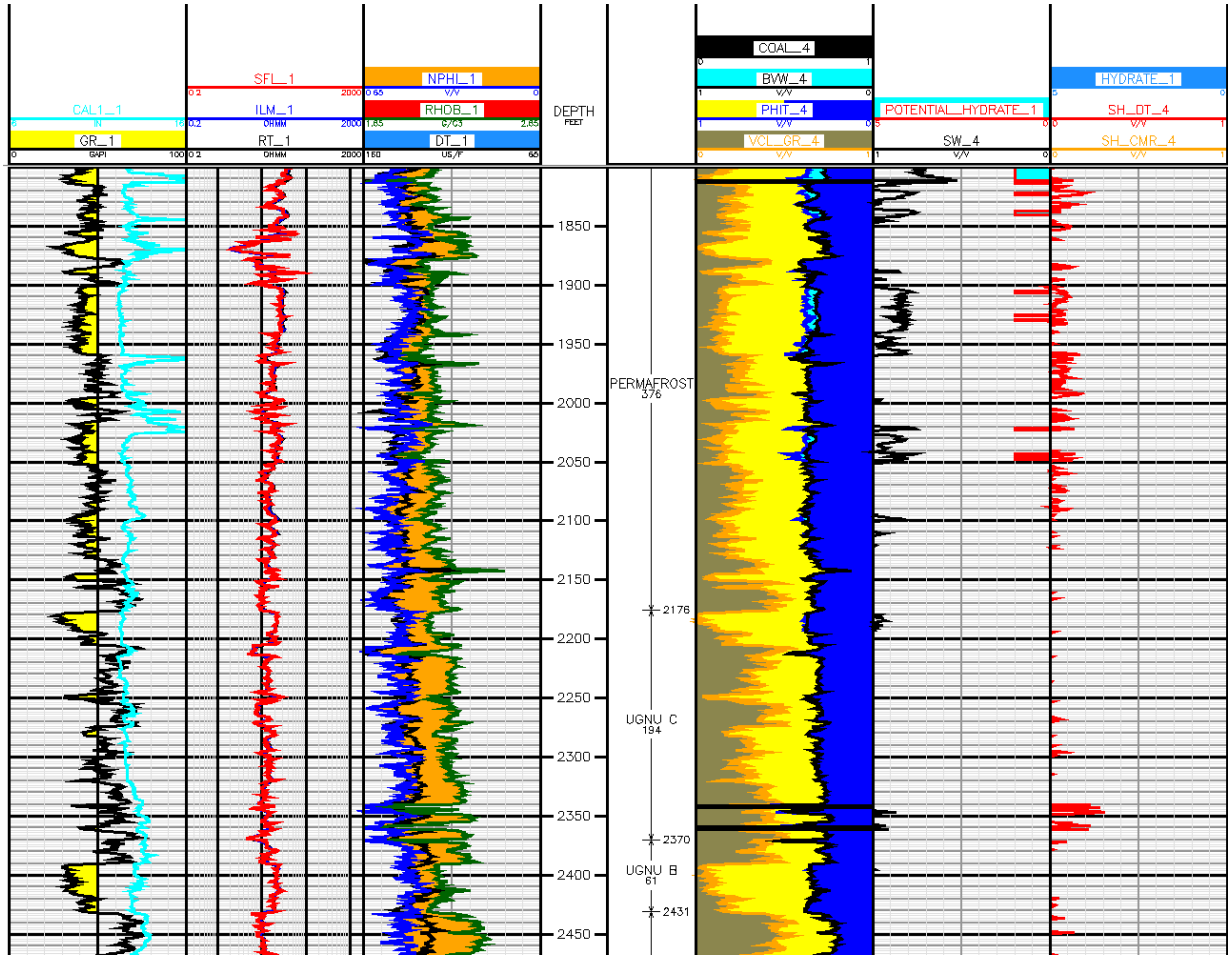

1. Shows a minimal amount of false hydrate with no classic hydrate response. There is no gas hydrate identified in this well.

1C-05

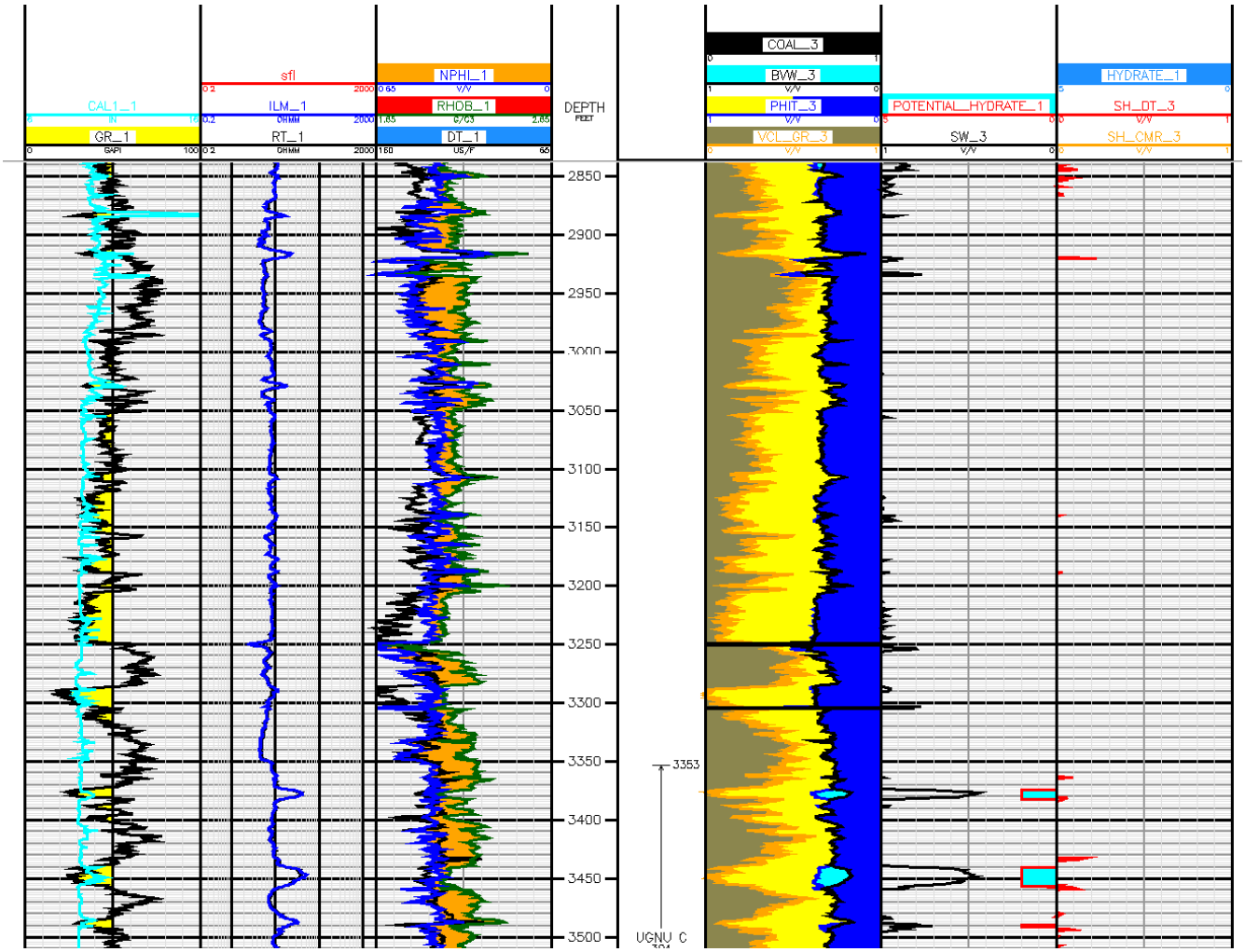

1. No hydrate indicated until the Ugnu interval, which does not contain hydrates.

HOT ICE:

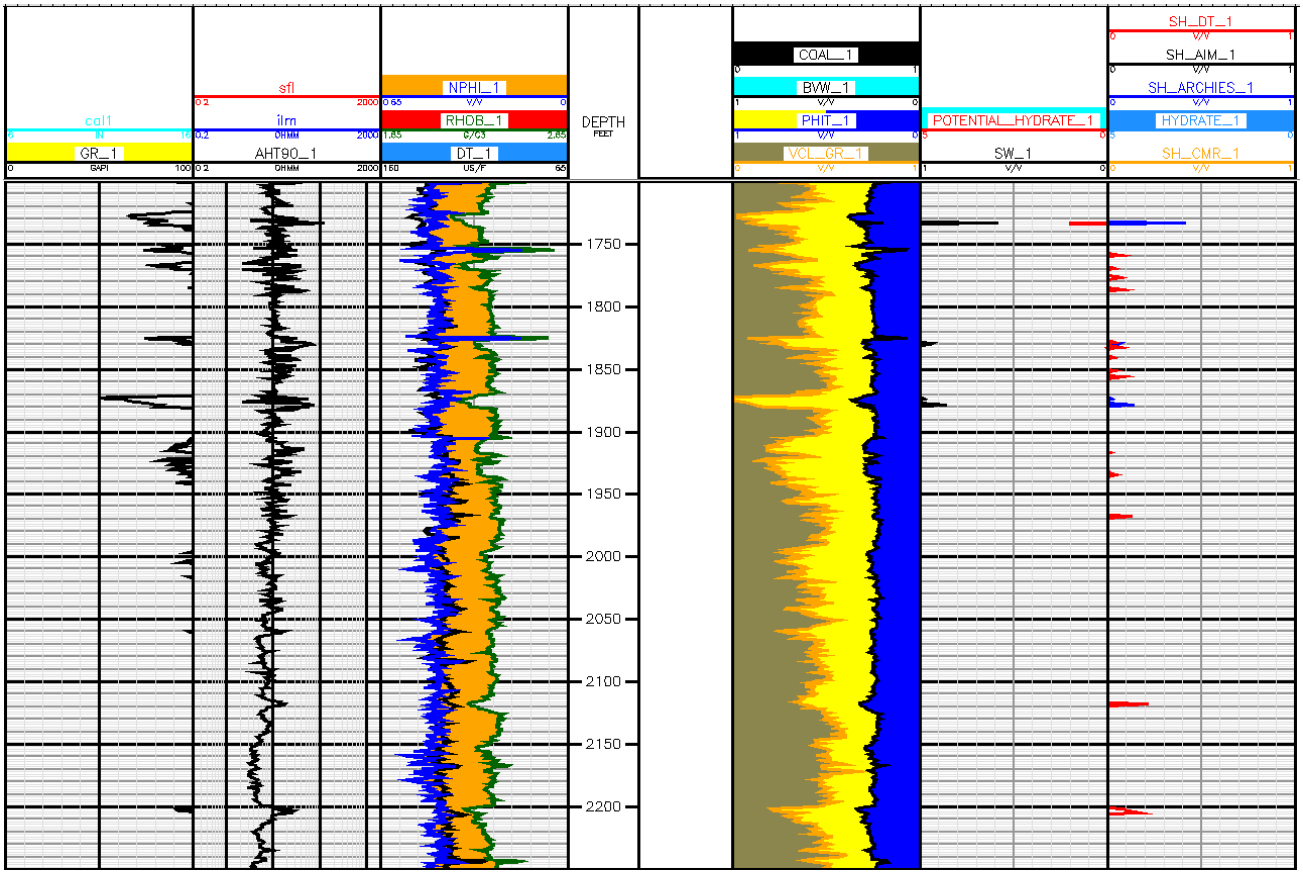

1. No hydrate indicated by the hydrate saturation module.

National Energy Technology Laboratory

626 Cochrans Mill Road
P.O. Box 10940
Pittsburgh, PA 15236-0940

3610 Collins Ferry Road
P.O. Box 880
Morgantown, WV 26507-0880

One West Third Street, Suite 1400
Tulsa, OK 74103-3519

1450 Queen Avenue SW
Albany, OR 97321-2198

2175 University Ave. South
Suite 201
Fairbanks, AK 99709

Visit the NETL website at:
www.netl.doe.gov

Customer Service:
1-800-553-7681